

SPIRE STM optical alignment campaign Photometer cold stop pupil imaging verification

KD, 18/11/2003
LAM.LOOM.SPI.NOT.031024 Ind 1 Rev 0

Reference documents

- RD1 "Photometer C.S.-tool" drawing SPI-OAL-30-DD-01-A, 07-08--2002.
 RD2 K. Dohlen, "Herschel-SPIRE: Optical error budgets", LOOM.KD.SPIRE.2000.002-4, 17/1/2002.
 RD3 Y. Alanou, "Alignment Tools Specifications", LOOM. YA. SPIRE. 2002.001.05, 26/08/2002.

Introduction

The SPIRE alignment plan provides pupil quality verification by observation of the projected cold stop tool onto the M2 tool. Four holes along the M2 tool edge are equipped with slits indicating the edge of the telescope pupil, see Fig. 1. The slits correspond nominally to slits in the CS tool. The coincidence of the slits is observed - using a specially designed Loupe - for five different points in the FOV (centre and corners).

The full nominal pupil imaging verification procedure was not applied to the STM instrument because of severe misalignment of some mirrors (CM3 in particular) and because of erroneous definition of the cold stop tools. Sufficient measurements were made however, partly by different means, to be able to estimate the pupil imaging quality.

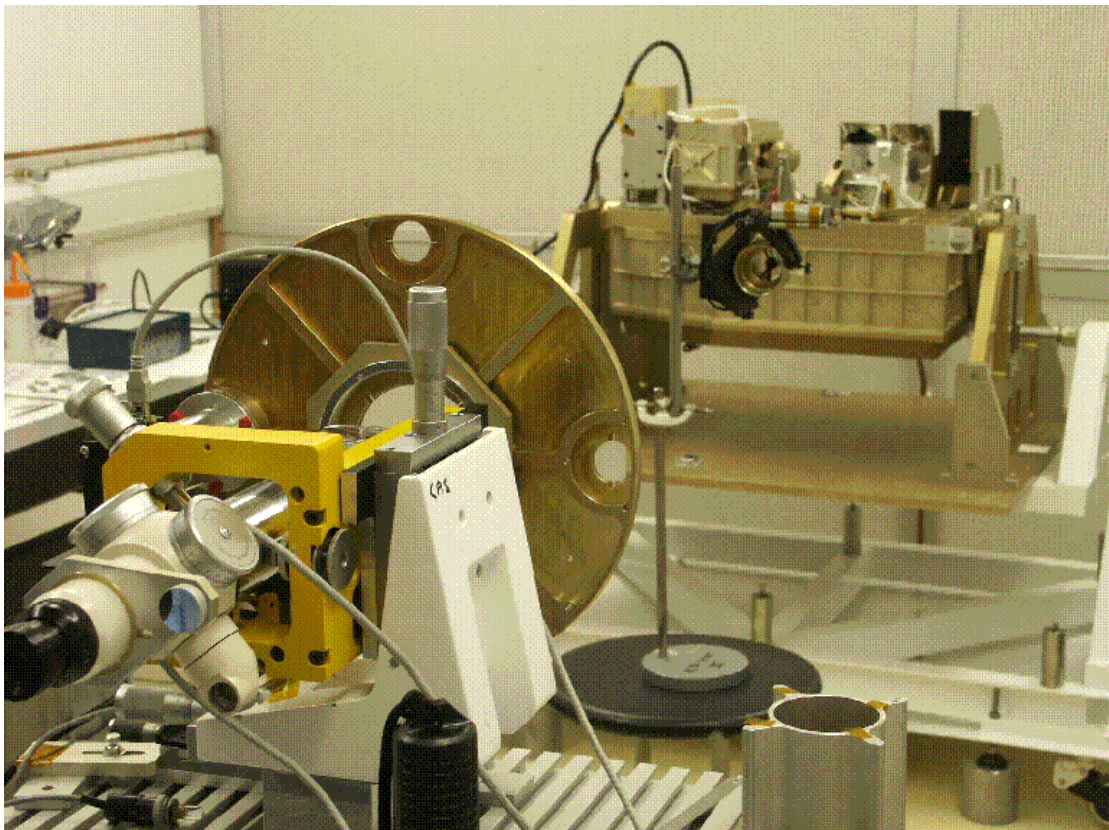


Figure 1. Setup of the M2-tool in front of the SPIRE instrument system.

Pupil magnification

Pupil magnification of the theoretical system and the as-built STM system are compared, see Table 1. For the theoretical system, magnification is calculated from ray tracing data (bolpht155d_M2tool). For the as-built STM system, magnification was calculated from PCS tool dimensions (detail of drawing [RD1] shown in Figure 2) and dimensions of its shadow projected onto the M2 tool (Fig. 3). The PCS tool was projected onto the M2 tool by placing a strong light source (fibre) in the SLW detector position. The shadow was drawn on a sheet of paper from which measurements are made using a ruler.

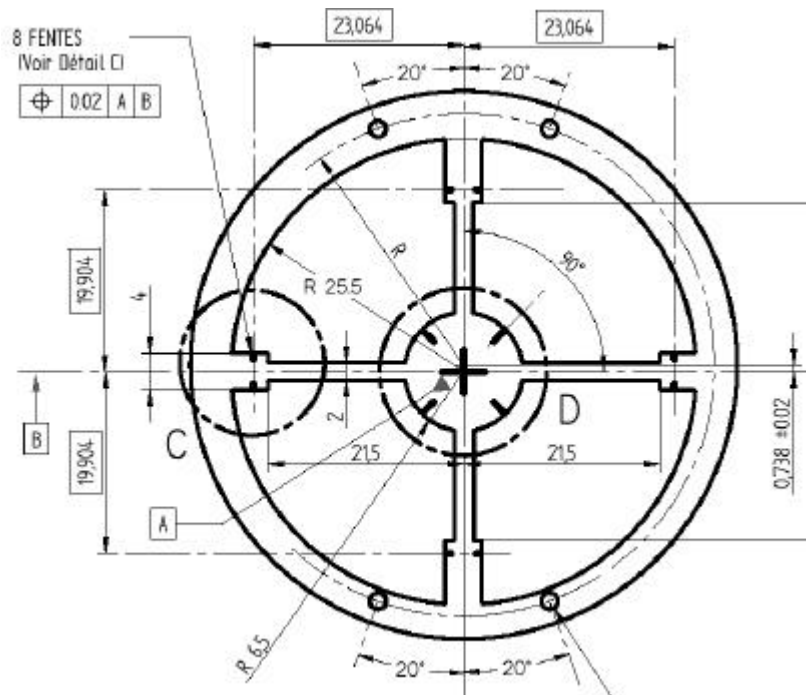


Figure 2. Facsimile of the photometer cold stop tool drawing.

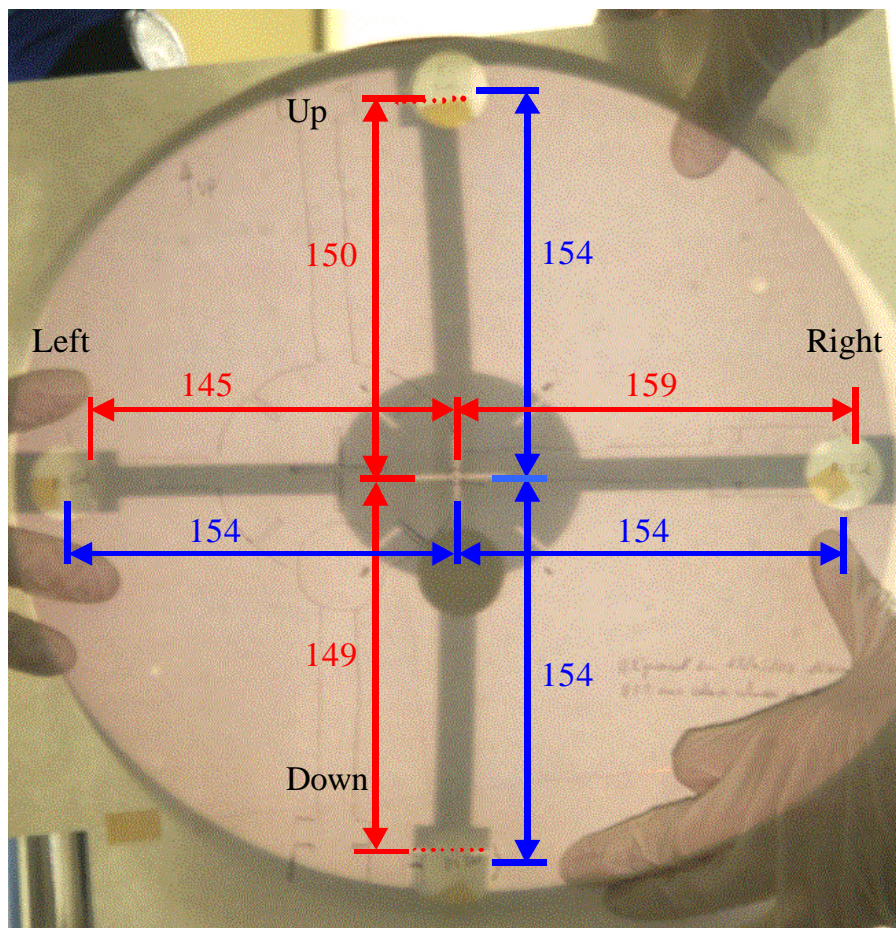


Figure 3. Shadow of the PCS tool projected onto the M2 tool. For clarity, a sheet of paper is held in front of the M2 tool, but the four holes around the edge of the tool indicating the edge of the telescope pupil are seen by transparency. The shadow seen here is obtained after readjustment of the M2 tool so that its centre coincides with the central cross of the PCS tool. The pencil trace on the paper shows the original PCS tool shadow obtained with the M2 tool aligned according to the theoretical instrument gut ray. The darker spot below the central cross is due to the central hole in the BSM mirror, offset by the insertion of a 4mm shim under its feet.

The results of Table 1 show that the magnification is different at different positions around the pupil: Larger horizontally than vertically, and larger Left than Right. Up and Down have the same theoretical magnification; this is to be expected since the system is symmetrical about the horizontal plane.

The measured and theoretical results correspond well for the Left and Right values. They are within 0.5% of each other, corresponding to an error at the M2 plane of 0.7mm. The results do not correspond so well for the Up and Down values, however. Here the difference between theory and measurements is around 2%, corresponding to 3mm at M2 (0.5mm at the CS).

The precision of the measured parameters is between ± 0.5 and ± 1.0 mm in the M2 plane, mainly due to lack of sharpness in the projected shadow, imprecision in the shadow drawing, and imprecision of the ruler-based measurement. While the Left/Right results are within this error estimate, the Up/Down results are significantly larger.

Known error sources not taken into account in this analysis include:

- Erroneous M2 distance: The M2 tool was set at a distance of 2999mm from the LAM-HOB reference plate. This distance was calculated for the cold instrument design. Its correct warm value is 3011.44mm. The error in projected pupil dimension due to this error is $12.44/(2*8.68) = 0.7$ mm, equal in all directions.
- Mirror orientation errors: The orientation error of CM3 of 27' is estimated to give an anamorphic error due to the increased angle between the M2 tool and the gut ray of about 0.5mm. Errors of a few arcminutes are assumed to be negligible.
- Mirror surface errors: It can be seen that mirrors coinciding with the pupil (CM4) or with the image (PM6) cannot influence the pupil magnification. Mirrors concerned are therefore CM3, CM5, PM7, PM8. Errors in Radius of curvature and toricity of these mirrors will give rise to both overall and anamorphic pupil magnification errors and this is likely to be the prominent cause of the discrepancies noted.

An error of 3mm is compatible with the pupil alignment error budget [RD2] (residual pupil aberrations of the optical design: 7.7mm, instrument internal alignment: 6.2mm). Moreover, since the actual magnification is smaller than the theoretical magnification, the projected cold stop will under-fill M2, hence producing a loss of astronomical signal, but not increasing stray light from the M2 surround.

Table 1. Parameters and results of pupil magnification calculations.

			Left	Right	Up	Down
<i>Theoretical</i>						
	PCS dimension	(mm)	21.0608	-19.1819	-23.2996	23.2996
	M2 projection	(mm)	154.06	-154.06	-154.06	154.06
	Magnification (Mt)		7.32	8.03	6.61	6.61
<i>Measured</i>						
	PCS dimension (drawn)	(mm)	19.904	-19.904	-23.064	23.064
	M2 projection	(mm)	145	-159	-150	149
	Magnification (Mm)		7.28	7.99	6.50	6.46
<i>Comparison</i>						
	dM/M = (Mm-Mt)/Mt		-0.41%	-0.54%	-1.64%	-2.30%
	dR = R dM/M	(mm)	-0.63	0.83	2.53	-3.54

Pupil aberrations

Pupil aberrations are measured by observing the shadow of the slits machined into the CS tool at the pupil edge as seen through the holes with corresponding slits in the M2 tool. This observation is made possible by the use of a specially designed Loupe interfaced with a CCD camera, see Figure 4. Figure 5 shows images taken for four positions in the FOV, three corners (A, B, C) and the centre (E), see Figure 6. The fourth corner (D) was unavailable because of a faulty LED. The image corresponding to field point E indicates the orientation of the images and illustrates the method used for analysis of the images:

- Image scale (mm/pixel) is determined by considering the M2-tool hole diameter.
- Position of the M2-tool is given by point P
- Position of the CS-tool shadow is given by point Q
- Pupil aberrations are the variations in the difference between the coordinates of P and Q.

For a correctly manufactured CS-tool, the difference between P and Q would be expected to be close to zero for image point E (taking account of the gap between the CS-tool shadow and the M2 tool edge). This is clearly not the case due to CS-tool

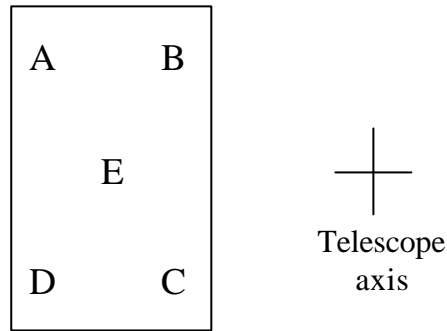


Figure 6. Definition of D-tool sources as seen by observing the instrument input focal plane from the M2 tool.

Table 2. Theoretically expected pupil aberration (design residual) compared with measured results. Left, Right, Up, Down corresponds to the four measurement positions around the M2 edge. Field points A, B, C, D, and E correspond to the five image plane (D-tool) sources. For the STM, measurements were done only for the Right measurement position. For the PFM, this table should be completed.

			Left		Right		Up		Down	
<i>Theoretical</i>			Zspire	Yspire	Zspire	Yspire	Zspire	Yspire	Zspire	Yspire
	Field point A	(mm)	-3.53	-2.09	2.69	2.57	3.43	3.60	-3.88	-5.28
	Field point B	(mm)	-0.51	1.20	1.83	1.05	2.39	1.10	-0.51	-0.77
	Field point C	(mm)	-3.53	2.09	2.69	-2.57	-3.88	5.28	3.43	-3.60
	Field point D	(mm)	-0.51	-1.20	1.83	-1.05	-0.51	0.77	2.39	-1.10
	Field point E	(mm)	0.00	0.00	0.00	0.00	0.00	0.00	0.00	0.00
<i>Measured</i>										
	Field point A	(mm)			3.70	2.18				
	Field point B	(mm)			1.02	1.53				
	Field point C	(mm)			1.60	-1.91				
	Field point D	(mm)								
	Field point E	(mm)			-0.50	-0.80				
<i>Difference</i>										
	Field point A	(mm)			1.01	-0.40				
	Field point B	(mm)			-0.82	0.49				
	Field point C	(mm)			-1.09	0.67				
	Field point D	(mm)								
	Field point E	(mm)			-0.50	-0.80				
<i>Error (length of difference vector)</i>										
	Field point A	(mm)		NA	1.09	NA		NA		NA
	Field point B	(mm)		NA	0.95	NA		NA		NA
	Field point C	(mm)		NA	1.28	NA		NA		NA
	Field point D	(mm)		NA		NA		NA		NA
	Field point E	(mm)		NA	0.94	NA		NA		NA
	<i>Mean error</i>	(mm)		NA	1.06	NA		NA		NA

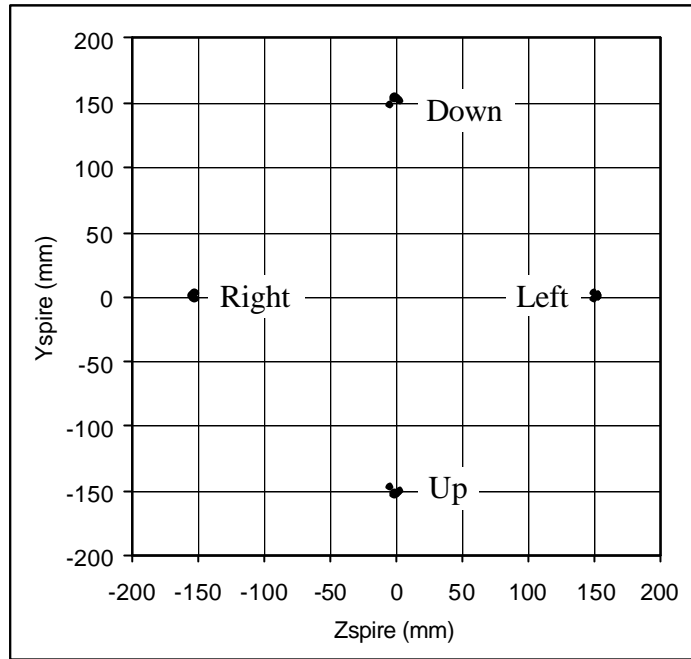


Figure 7. To scale view of the expected pupil aberrations at the four holes of the M2 tool.

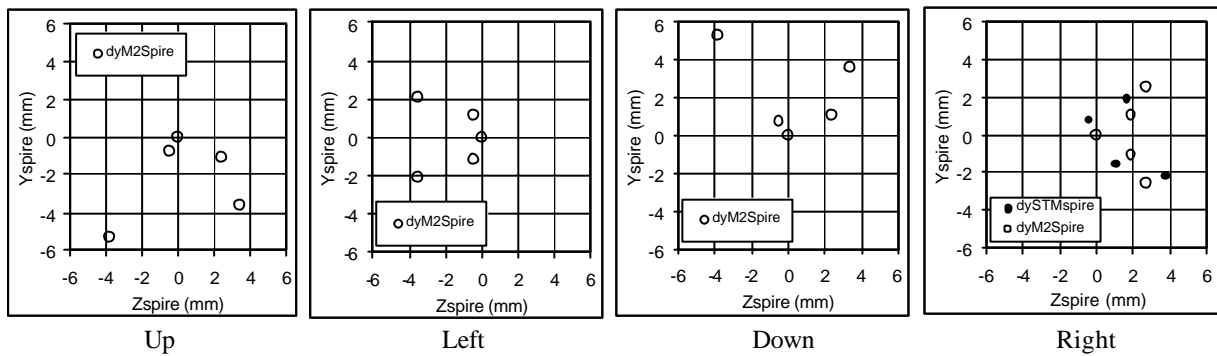


Figure 8. Enlarged views of the pupil aberrations at each of the M2-tool holes. Open circles are theoretical values, filled circles are measurement results (Right only).

Conclusion

Pupil magnification is found to have very good agreement with theory in the horizontal plane, but a discrepancy corresponding to an error of 3mm in the M2 plane, has been found in the vertical plane. Probably due to radius of curvature and toricity errors of certain mirrors, this error is compatible with the instrument error budget.

Pupil aberrations have been measured at one position along the M2 edge. Good agreement with theoretical values have been found.

SPIRE STM optical alignment campaign 1: Photometer cold stop alignment verification

KD, 23/5/2003

Reference documents

- RD1 G. Rousset, "HERSCHEL-SPIRE, SPIRE STM MIRRORS, Optical measurement report", LAS.QUA.SPI.PR.V.030024 Iss1 Rev0, 31/03/2003.
- RD2 "Photometer C.S. -tool" drawing SPI-OAL-30-DD-01-A, 07-08--2002.
- RD3 K. Dohlen, "Herschel-SPIRE: Optical error budgets", LOOM.KD.SPIRE.2000.002-4, 17/1/2002.

Introduction

Measurements on mirrors have shown that some of them suffer from several minutes of misalignment between the optical surface normal and the mounting spigot. In order to measure the effect of these errors and determine whether other error sources were also contributing, the induced deviation of the gut ray was measured by projecting the PCS tool onto the M2 tool by placing a strong light source (fibre) in the SLW detector position. Figure 1 shows this setup and Figure 2 shows the projected shadow.

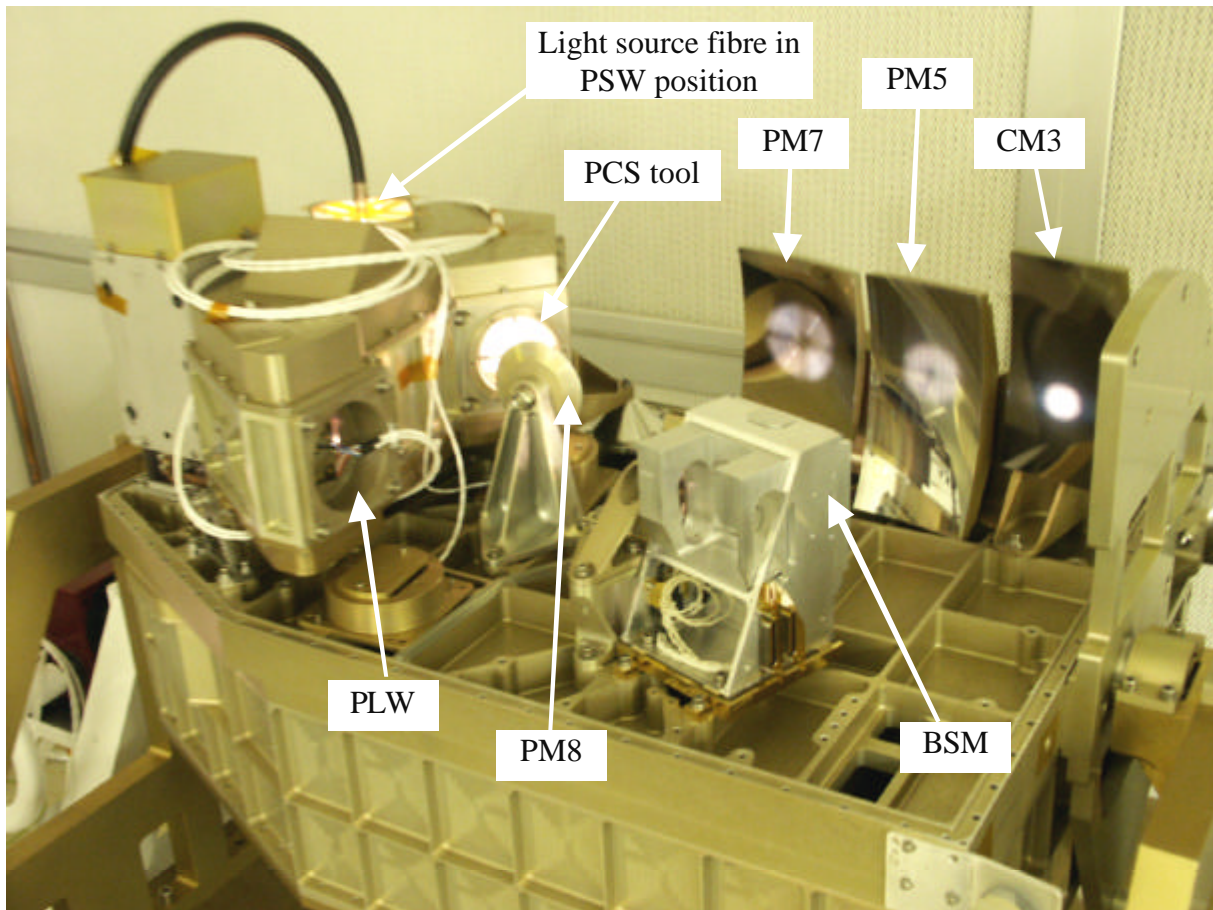


Figure 1. Setup of the PCS projection system. The fibre pipes light into the PSW detector position. Pupil outlines are clearly seen on all mirrors.

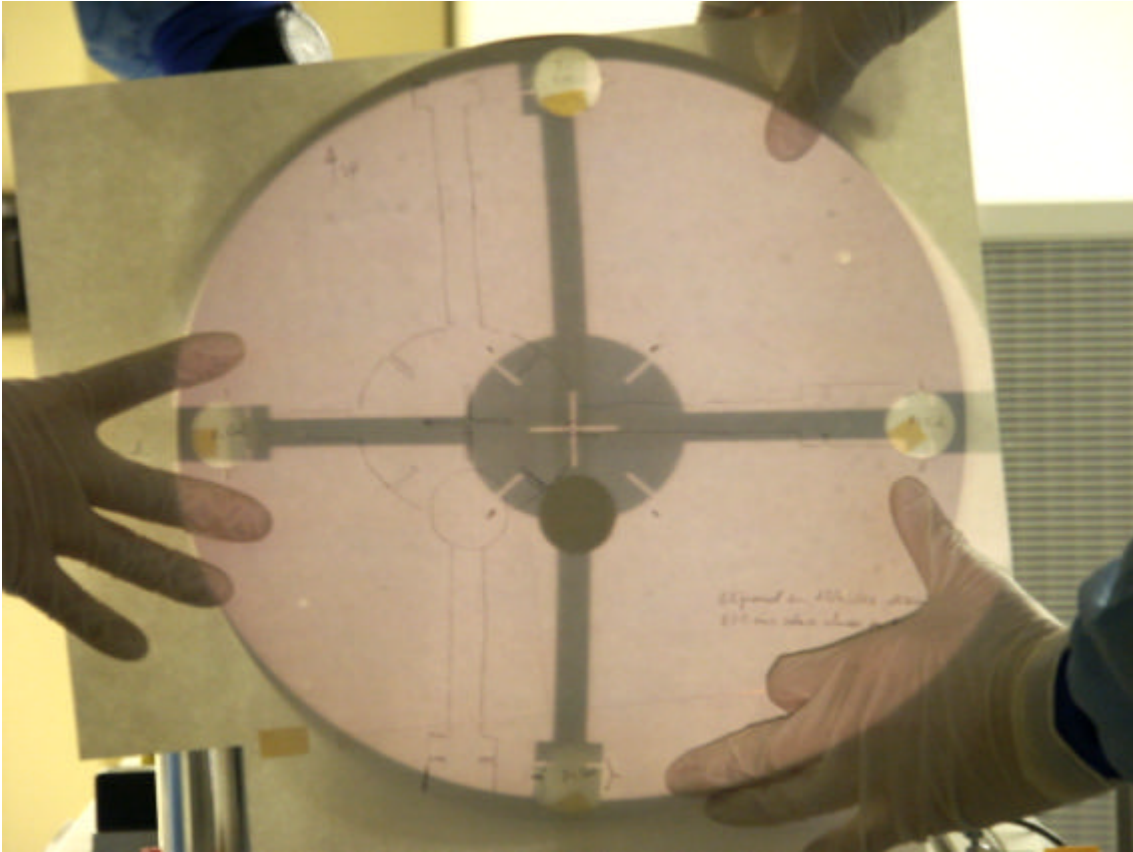


Figure 2. Shadow of the PCS tool projected onto the M2 tool. For clarity, a sheet of paper is held in front of the M2 tool, but the four holes around the edge of the tool indicating the edge of the telescope pupil are seen by transparency. The shadow seen here is obtained after readjustment of the M2 tool so that its centre coincides with the central cross of the PCS tool. The pencil trace on the paper shows the original PCS tool shadow obtained with the M2 tool aligned according to the theoretical instrument gut ray. The darker hole below the central cross is due to the central hole in the BSM mirror, offset by the insertion of a 4mm shim under its feet.

Analysis

The deviation of the projected PCS tool central cross and the centre of the M2 tool is $\Delta Z = 46.8\text{mm}$ along the SPIRE Z axis (oriented towards PAX) and $\Delta Y = -4.0\text{mm}$ along the SPIRE Y axis (oriented towards the spectrograph).

Table 1 gives measured angular deviations, Θ_Z and Θ_Y , of the mirror surface for each mirror in the photometer optical train. The values are obtained from RD1.

An error has also been detected in the definition of the photometer cold stop tool (PCS tool, RD2). The central PCS tool reticle has been drawn centred in the elliptical CS aperture while it should have been located centred within the circular CS interface. This gives a decentering of 0.738mm along the Z axis (parallel with the SPIRE bench).

Z_{sens} and Y_{sens} represent the sensitivity of pupil centration on M2 for tilt of each mirror and decentering of the cold stop, obtained by raytracing (SpirePhotTol30.XLS). Z_{pup} and Y_{pup} are corresponding pupil centration errors.

The total theoretical pupil deviation obtained by summing the individual errors is $\text{Sum}Z_{\text{pup}} = 45.313\text{mm}$ and $\text{Sum}Y_{\text{pup}} = 3.120\text{mm}$. This is within 1.7mm of the observed pupil deviation, corresponding to a residual relative pupil alignment error of 1.1% . This has been verified by introducing all the errors simultaneously in a raytracing model (BolPhtRev21_STM). Figure 3 shows plot of the theoretical instrument gut ray impact on M2 overlaid on the photo of the PCS tool projection.

Table 1. Measured mirror tilt errors and cold stop decentering error, and their effect on pupil alignment.

Subass'y	Mirror	ThetaZ	ThetaY	Zsens	Ysens	Zpup	Ypup
Fore optics		arcmin	arcmin	mm/arcmin	mm/arcmin	mm	mm
	CM3	-27.19	7.90	-1.581	1.519	42.99	12.00
	CM5	-0.90	3.60	1.461	-1.441	-1.31	-5.19
Photometer							
	PM6	3.00	-5.30	-0.949	0.858	-2.85	-4.55
	PM7	0.50	-0.70	1.71	-1.163	0.86	0.81
	PM8	0.00	0.20	-0.314	0.202	0.00	0.04
	PCS (mm)	0.74	0.00	7.631	6.583	5.63	0.00
	PM9	0.20	0.00	0.005	-0.014	0.00	0.00

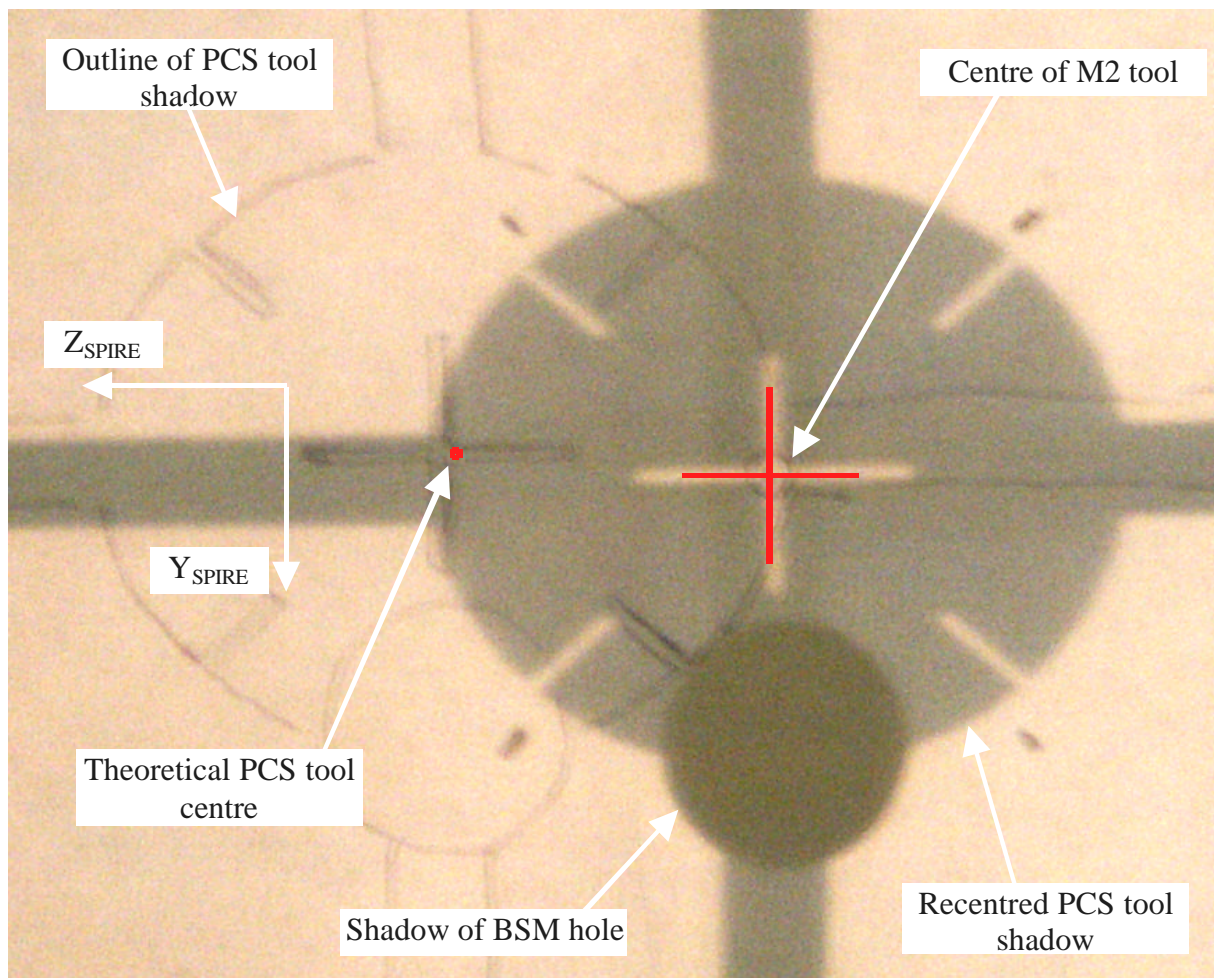


Figure 3. Detail of the PCS tool shadow on the M2 tool with theoretical raytracing result superimposed (red). Scale ~1:1.

Conclusion

We attribute the remaining 1.1% (1.7mm) pupil alignment error to perturbations in the SPIRE structure. This is well within the SPIRE error budget [RD3] allocation of 4.0% (6.2mm) internal instrument alignment error and 2.6% (4.0mm) external instrument alignment, indicating that the manufacture of the SPIRE structure is highly accurate.

When the excessive errors in CM3, PM5 and PM6 are corrected, the instrument will be well within its budget.

SPIRE STM optical alignment campaign

Photometer Hartmann test

KD, 11/9/2003

1. Reference documents

- RD1 G. Rousset, "HERSCHEL-SPIRE, SPIRE STM MIRRORS, Optical measurement report", LAS.QUA.SPI.PRIV.030024 Iss1 Rev0, 31/03/2003.
- RD2 "Photometer C.S.-tool" drawing SPI-OAL-30-DD-01-A, 07-08--2002.
- RD3 K. Dohlen, "Herschel-SPIRE: Optical error budgets", LOOM.KD.SPIRE.2000.002-4, 17/1/2002.
- RD4 K. Dohlen, "Herschel-SPIRE: Analysis of 3-D measurements of CM3", 15/4/2003.

2. Introduction

Measurement of SPIRE image quality is done using a Hartmann test, see Fig. 1. A tool holding a grid of point sources (D-tool) is placed in the position of one of the detectors. A mask containing a grid of holes is placed in the instrument's internal cold stop pupil (Hart tool). A lunette containing two lenses and a CCD camera is placed in front of the instrument entrance (Hartmann lunette). The lunette provides a telecentric image of the D-tool source and the CCD can be placed at different positions before (intra focal) and after (extra focal) the focal plane of the lunette. In extra and intra focal images, distorted images of the Hart tool grid is observed. Determining the position of each point in the grid allows calculation of the wavefront slope, hence quantitative determination of image quality.

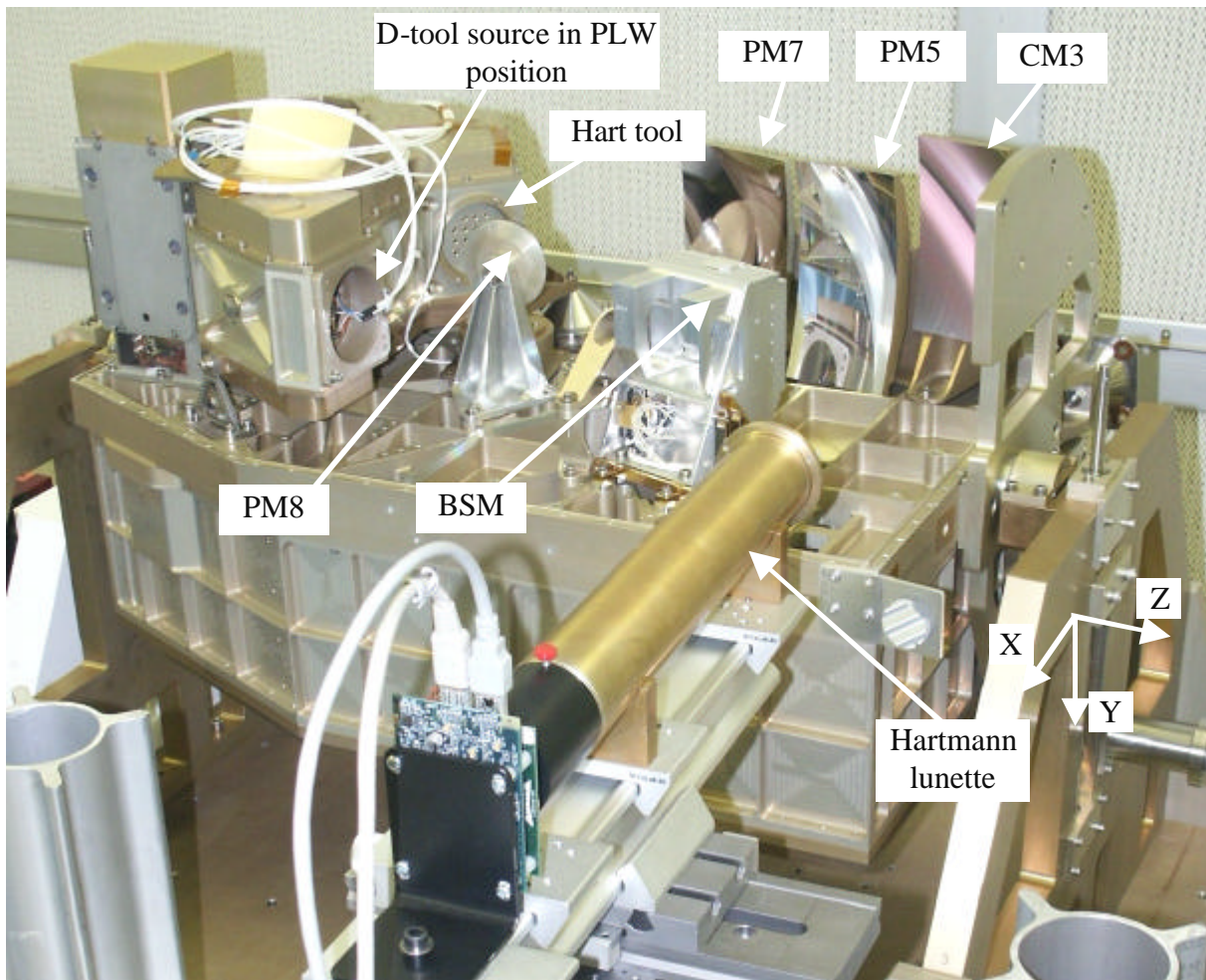


Figure 1. Setup of the Photometer Hartmann test. .

3. Coordinate axes

An image was taken of the projection of the PHart tool onto the M2 tool, see Figure 2. To get sufficient intensity, the D tool was replaced with the fiber fed light source. This image allows determination of the axes of the extra and intra focal images, thanks to the left/right asymmetries observed in the pattern of spots, and to the partial shadowing of one of the PHart holes by the hole in the BSM mirror.

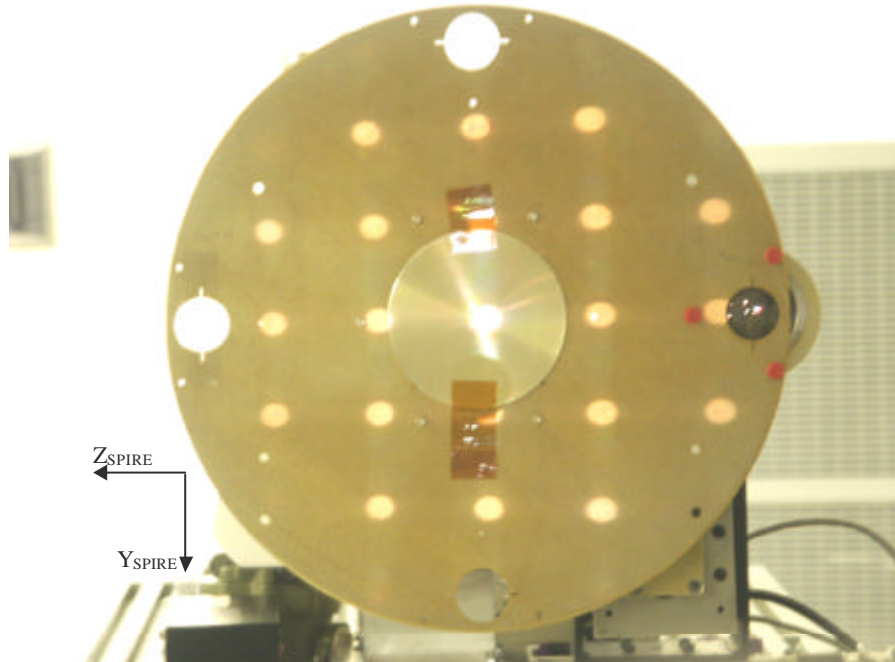


Figure 2. Shadow of the Photometer Hartmann (PHart) tool projected onto the M2 tool. The shadow seen here is obtained after readjustment of the M2 tool so that its centre coincides approximately with the central hole of the PHart tool.. The spot just below the central spot is partly covered by the central hole in the BSM mirror, offset by the insertion of a 4mm shim under its feet.

Figure 3 shows images obtained with the Hartmann lunette for the central D-tool source (a and b), and a comparison of the positions of PHart holes in the M2 plane as estimated from Figure 2 (circles) and as calculated from the slopes deduced from the Hartmann test (dots). Good agreement is found.

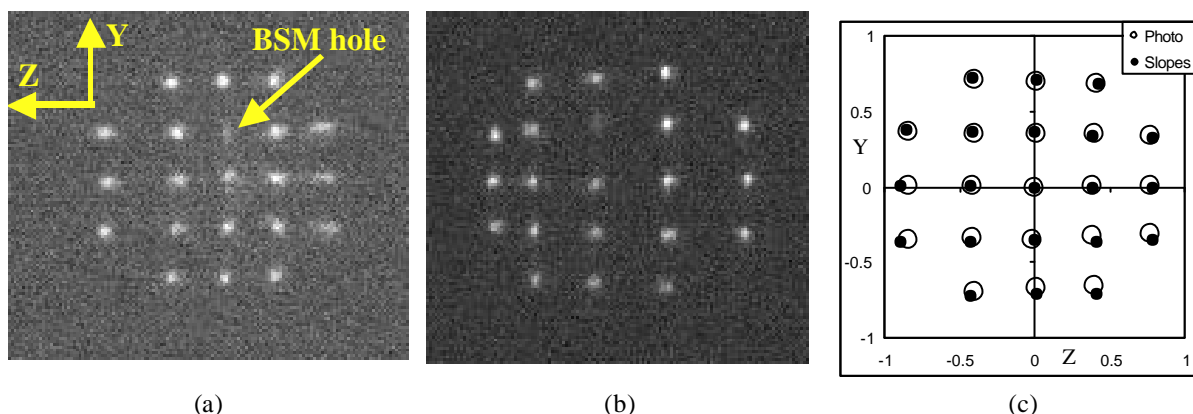


Figure 3. Images obtained with the Hartmann lunette for the central D-tool source (a and b), and a comparison (c) of the positions of PHart holes in the M2 plane as estimated from Figure 2 (circles) and as calculated from the slopes deduced from the Hartmann test (dots).

4. Setup and calibration

Before setting up the Hartmann bench in front of the SPIRE camera, it was pointed towards a well-defined object allowing calibration of the detector position on the Hartmann bench. Figure 4 illustrates the parameters involved. The object was placed at the nominal front focal distance (FFD, measured from the front flange of the Hartmann lunette) of $FFD = 310\text{mm}$, and the detector slide was adjusted for optimal sharpness of the object (Figure 5). The detector slide position (measured to the back edge of the detector slide) was then $a+b+c = 472\text{mm}$. The reference slide was placed such that the distance from its back edge to the detector slide back edge was $c = 100\text{mm}$. This distance is measured by the aid of a metallic ruler, and a piece of aluminium added to the reference slide eases this operation. Intra and extra focal distances are measured as deviations from $c = 100\text{mm}$. The position of the bench with respect to the instrument is most easily measured from the front edge of the front slide whose position is given by $a = 49.5\text{mm}$.

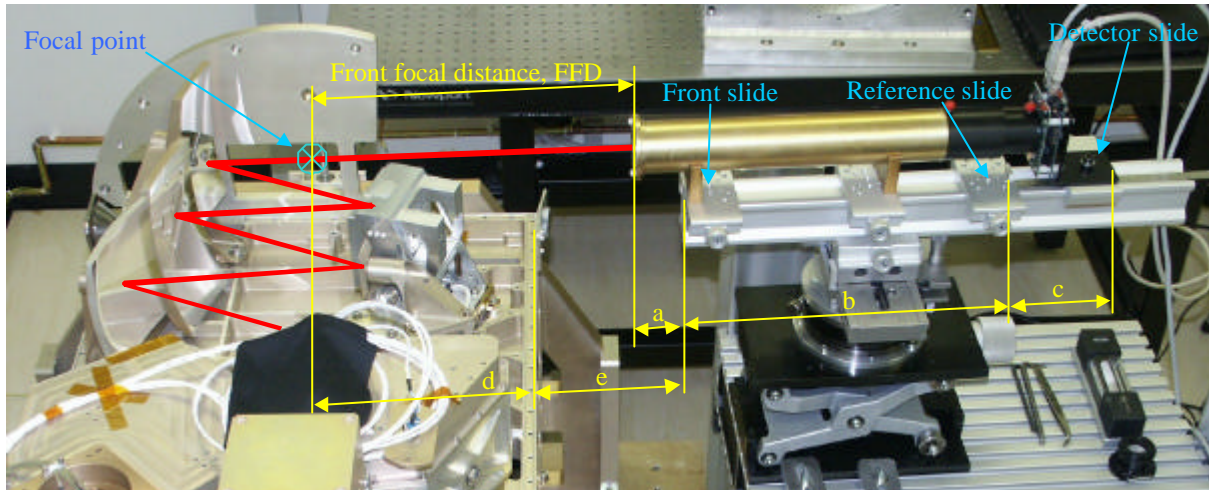


Figure 4. Parameters involved in the axial alignment of the Hartmann bench.

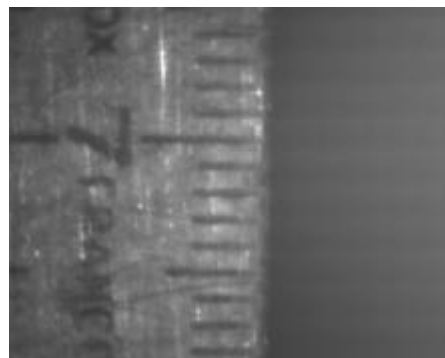


Figure 5. Image of the reference object used for focus calibration of the Hartmann bench.

The Hartmann bench was then turned towards the instrument as seen in Figure 4. Transverse alignment with the gut ray was done using the MAT. Axial alignment was done by measuring by the aid of a ruler the distance e from the edge of the SOB to the edge of the front slide of the Hartmann bench. Care was taken to measure this distance along the direction of, and directly below, the gut ray. The value of e was obtained as:

$$e = FFD + a - d$$

where $d = 1.00415 d_C$ and $d_C = 215.43$ is the position of the focus in the instrument at 4K, determined by raytracing (Figure 6). Hence $e = 310 + 49.5 - 1.00415 * 215.43 = 143.18$.

Due to some erroneous inputs, the value of e assumed during the tests was 143.8. The precision of the adjustment was estimated to $\pm 0.5\text{mm}$.

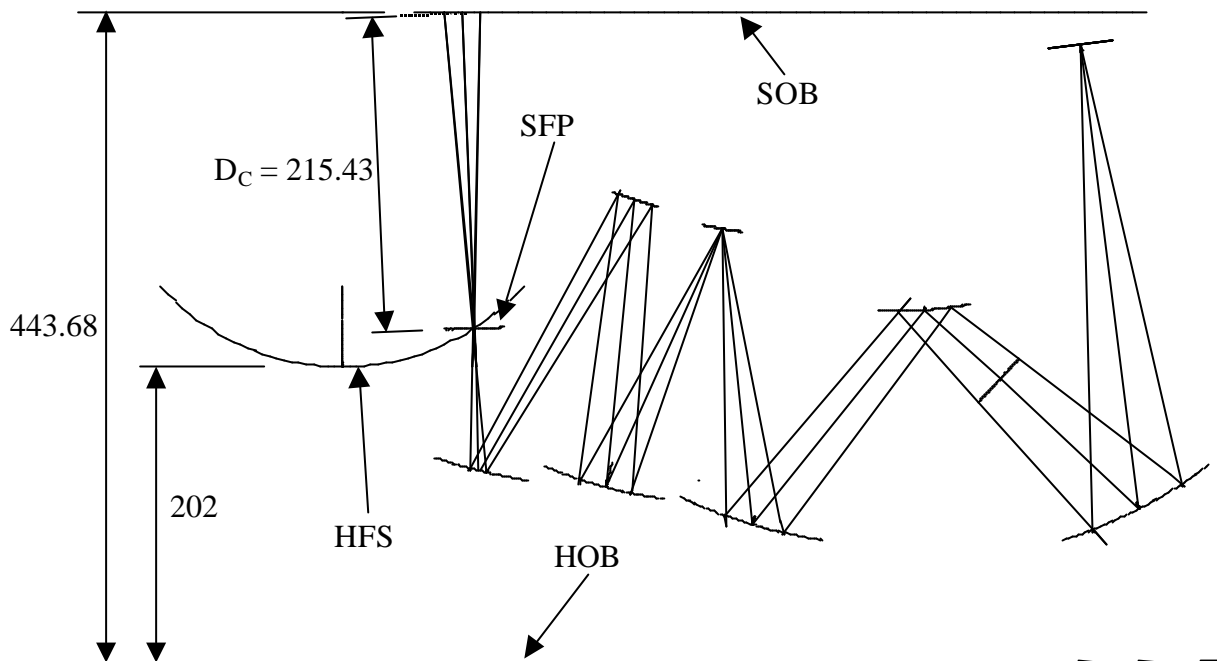


Figure 6. Raytrace model (BolPhtRev25) used to determine the position of the focal plane with respect to the upper edge of the SOB. All dimensions are cold (4K). HOB: Herschel optical bench, SOB: upper edge of the Spire optical bench, HFS: Herschel focal surface, SFP: Spire focal plane, perpendicular to the gut ray at the best focus of the centre of the photometer field.

Lateral alignment to the gut ray using the MAT assures pointing towards the central LED in the D-tool (E). In order to point towards the other LEDs, located in the four corners and named A, B, C, D, lateral shifts and tilts of the Hartmann bench are effectuated. Figure 7 shows a view of the instrument where the field points are defined as projected onto the instrument input plane. Table 1 indicates the adjustments to be done to the Hartmann bench, calculated from outputs from the raytracing model (BolPht155d). Figure 8 defines the Hartmann bench adjustment parameters.

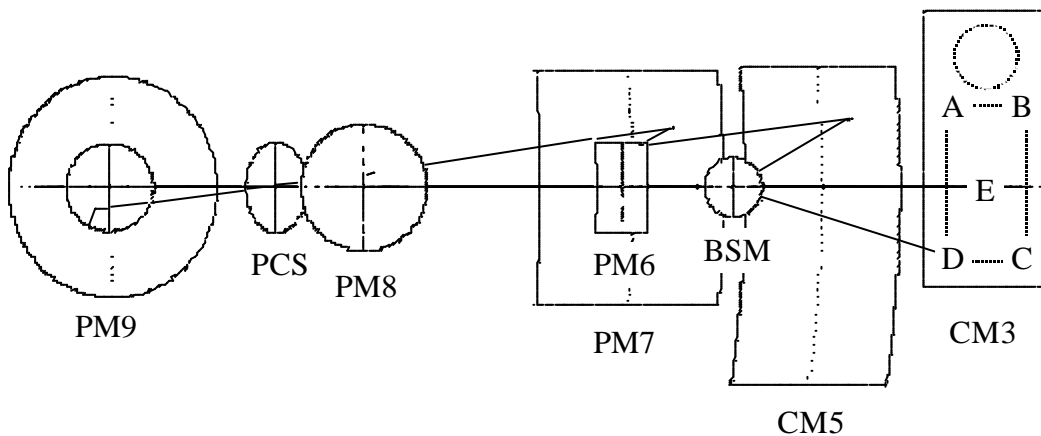


Figure 7. Definition of field points as projected onto the SPIRE input plane.

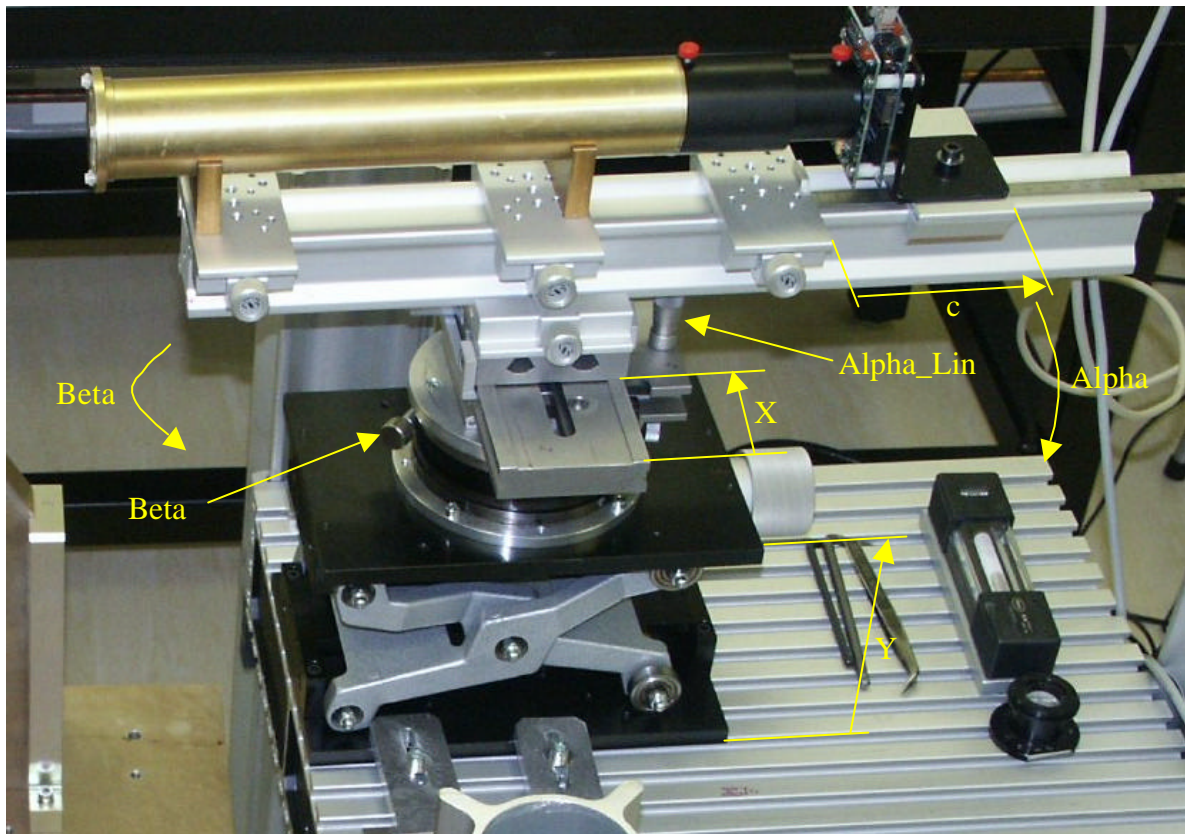


Figure 8. Definition of Hartmann bench adjustment parameters.

Table 1. Calculation of Hartmann bench adjustment parameters for each field point.

Parameter	Unit	E	A	B	C	D
<i>Synopsis input</i>						
H	arcmin	0.00	-2.00	2.00	2.00	-2.00
G	arcmin	0.00	-4.00	-4.00	4.00	4.00
<i>Synopsis output</i>						
tan_beta		0.000000	-0.006301	0.006286	0.006286	-0.006301
tan_alpha		0.000000	-0.012575	-0.012573	0.012573	0.012575
<i>Linear Hartmann bench coordinates</i>						
deltaX	mm	0.00	-12.99	12.96	12.96	-12.99
deltaY	mm	0.00	-25.92	-25.91	25.91	25.92
<i>Angular Hartmann bench coordinates</i>						
deltaBeta_dms	deg:min:sec	-0:0:0	-0:21:40	0:21:37	0:21:37	-0:21:40
deltaAlpha_dms	deg:min:sec	-0:0:0	-0:43:14	-0:43:13	0:43:13	0:43:14
<i>Linear Hartmann bench adjustments</i>						
X	mm	69.50	56.51	82.46	82.46	56.51
Y	mm	142.00	167.92	167.91	116.09	116.08
<i>Angular Hartmann bench adjustments</i>						
Beta_dms	deg:min:sec	130:30:0	130:8:20	130:51:37	130:51:37	130:8:20
Alpha_lin	mm	4.08	5.35	5.34	2.83	2.83

5. Data collection and reduction

Once set up for a given point in the field, corresponding to a LED in the D-tool, sliding the detector slide along the rail allows study of the evolution of the Hartmann grid during the passage through focus. Intra and extra focal images are normally taken at defocus distances of $\pm 15\text{mm}$, ie at $c_{\text{Intra}} = 85\text{mm}$ and $c_{\text{Extra}} = 115\text{mm}$. In case of excessive aberrations this can be increased. Images are saved as BMP files.

5.1. Detect and sort Hartmann points

An IDL program (HartApplic.pro, HartEvent.pro, HarTest.pro) is created, doing the following:

- 1) Read Extra focal image
- 2) Read Intra focal image. This image is rotated 180 degrees so that the grid points correspond
- 3) Subtract dark (if necessary)
- 4) Apply a softening filter (if necessary). May be applied several times for increased blurring/noise reduction.
- 5) Apply a threshold to obtain a binary image. The threshold level is adjusted in real time so as to have the required number of patches (21)
- 6) Detect the peak within each patch and sort the peaks
- 7) Write peak coordinates to a file

Figure 9 shows an image of the screen. Each action can be addressed separately via the File menu, except action 5, which is done interactively by the aid of slides. They can also be addressed in two groups via buttons: "DoAll" groups actions 1-4 and "Finish" groups actions 6 and 7. Additional filtering can be applied if necessary during the search for threshold. The filtered images are shown on the left and the threshold images are shown on the right. The number of patches found each time a new threshold level is set is printed in the IDL window. **This number should be 21.** Threshold level is in % of peak pixel intensity. Figure 9 shows the screen image when appropriate thresholds have been set, just before pushing the "Finish" button. Notice that although the hole in the BSM mirror blocks most of the Hartmann hole second from the top in the middle column, enough signal is received to define a patch at that point.

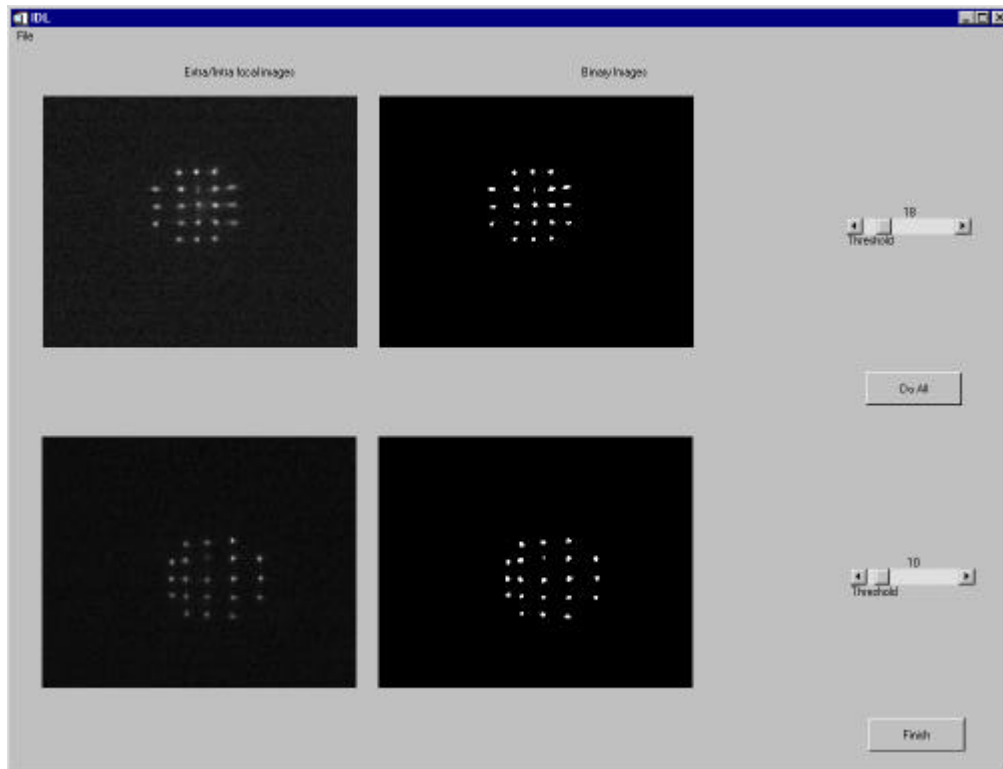


Figure 9. Screen shot of the IDL program for detection and sorting of Hartmann points.

5.2. Hartmann data reduction

The data file is imported into an XL file (Current version TraitImagHartTes32.xls) where it occupies a spreadsheet named typically "STM_PLW_E" for "Dtool diode E in PLW focal plane of the STM model". The XL file treats the data in two principal sheets:

5.2.1. Transverse aberrations: "HartNew"

The Hartmann test allows determination of the transverse aberrations of a system. These are habitually presented in the form of spot diagrams, and correspond to the first derivatives of the system wavefront. Determination of transverse aberrations is effectuated in the spreadsheet named "HartNew" and corresponds to the following main operations:

- Fetch peak coordinate data, units of pixels
- Centre and calculate coordinates in mm. Coordinate axes, labelled Z and Y, are oriented according to SPIRE convention.
- Calculate Z and Y ray slopes as the sum of corresponding extra and intra focal coordinates, divided by the distance between extra and intra focal image planes.
- From slopes, calculate the relative pupil coordinates of each grid point. This is compared with pupil coordinates measured from the photograph of Fig. 2, see Fig. 3.c.
- Calculate theoretical focus coordinates of the rays as they pass through the theoretical focal plane. This equals half the difference of corresponding extra and intra focal coordinates. Plotted in an X-Y plot, this gives the spot diagram to be compared with the theoretical spot diagrams produced by a raytracing program.
- Calculate through-focus spot diagrams by combining theoretical focus coordinates and slope values. Five focal positions are calculated and plotted, with adjustable defocus offset and defocus step.

If the parameter DetFlag = 0, then the spot diagrams are scaled to correspond to the F/8.68 telescope focus. If DetFlag = 1, then the scale corresponds to the F/5 instrument focus.

5.2.2. Wavefront aberrations: "ZernikeFit"

Estimation of wavefront errors from transverse aberrations can be done by two methods: Integration [Malacara, *Optical shop testing 2nd ed*, p. 385 (1992)] or by least squares fitting of Zernike polynomials [R. Cublaichini, *JOSA* 69, p. 972 (1979)]. The latter, developed for adaptive optics (AO) and referred to as the modal approach, was adapted here because of its relative simplicity of implementation and the usefulness of its output in terms of Zernike coefficients.

By this method, the actual transverse aberrations are compared with synthetic aberrations calculated from polynomial functions representing derivatives of the Zernike polynomials and a set of estimated Zernike coefficients. The estimate is improved by damped least squares optimization until the difference between transverse aberrations is minimized.

The following operations are included in the spreadsheet "ZernikeFit":

- Fetch the theoretical-focus ray coordinates from the "HartNew" sheet
- Calculate ray coordinates according to a list of Zernike coefficients using functional representations of the derivatives of the Zernike polynomials (defined in the "Macro" sheet)
- Calculate the RMS of the difference between actual and calculated ray coordinates,
- Using the "Solver" routine (a powerful least squares algorithm built in to EXCEL), the Zernike coefficients are optimized to give minimum RMS difference
- Reconstruct the wavefront using the original (non-derivative) Zernike polynomials (functional forms given in "Macros" sheet) on a high-resolution map. The calculations for this map are done in the sheet "WFmap".

The 14 Zernike modes included in our calculations are defined in Table 2 in their cartesian representation. This is equivalent to the more common radial representation, but makes differentiation easier. The first derivatives are also included, as well as the factor by which the Zernike coefficients are multiplied to give the WFE RMS contribution for each polynomial. Since Zernike polynomials are orthogonal, the RMS error of the reconstructed wavefront equals the RSS of the RMS coefficients.

Table 2. Definition of Zernike polynomials and their derivatives used in our calculations.

No	Name	RMS factor	Wavefront W	X differential $\frac{\partial W}{\partial x}$	Y differential $\frac{\partial W}{\partial y}$
1	TiltX	$1/\sqrt{4} = 0.50$	x	1	0
2	TiltY	$1/\sqrt{4} = 0.50$	y	0	1
3	Focus	$1/\sqrt{3} = 0.58$	$-1+2y^2+2x^2$	4x	4y
4	AstX	$1/\sqrt{6} = 0.41$	y^2-x^2	-2x	2y
5	AstY	$1/\sqrt{6} = 0.41$	2xy	2y	2x
6	ComaX	$1/\sqrt{8} = 0.35$	$-2x+3xy^2+3x^3$	$-2+3y^2+9x^2$	6xy
7	ComaY	$1/\sqrt{8} = 0.35$	$-2y+3x^2y+3y^3$	6xy	$-2+3x^2+9y^2$
8	Sph	$1/\sqrt{5} = 0.45$	$1-6y^2-6x^2+6y^4+12x^2y^2+6x^4$	$-12x+24xy^2+24x^3$	$-12y+24x^2y+24y^3$
9	Tri5X	$1/\sqrt{8} = 0.35$	$3xy^2-x^3$	$3y^2-3x^2$	6xy
10	Tri5Y	$1/\sqrt{8} = 0.35$	y^3-3x^2y	-6xy	$3y^2-3x^2$
11	Ast5X	$1/\sqrt{10} = 0.32$	$-6xy+8xy^3+8x^3y$	$-6y+8y^3+24x^2y$	$-6x+24xy^2+8x^3$
12	Ast5Y	$1/\sqrt{10} = 0.32$	$-3y^2+3x^2+4y^4-4x^4$	$6x-16x^3$	$-6y+16y^3$
13	Coma5X	$1/\sqrt{12} = 0.29$	$3x-12xy^2-12x^3+10xy^4+20x^3y^2+10x^5$	$3-12y^2-36x^2+10y^4+60x^2y^2+50x^4$	-24xy
14	Coma5Y	$1/\sqrt{12} = 0.29$	$3y-12x^2y-12y^3+10x^4y+20x^2y^3+10y^5$	-24xy	$3-12x^2-36y^2+10x^4+60x^2y^2+50y^4$

6. Results

For the STM photometer, only two points (of five foreseen: centre and four corners) were measured by the Hartmann test. The results from these tests have allowed the data reduction to be tested and adapted to real measurement data, and to draw some conclusions regarding the optical quality of the STM.

6.1. Reference system

To compare the results obtained by the Hartmann test with the optical model, a new raytracing model (BolPhot155d_InstrOnly) has been made, replicating the conditions of the test setup:

- The telescope is removed: the test only concerns the instrument optical train
- The curved input focal plane is replaced by a flat input surface, coinciding with the telescope focal surface at the centre of the Photometer FOV and perpendicular to the gut ray: this corresponds to applying only transverse adjustments to the Hartmann lunette as described above.

Figure 10 shows through-focus spot diagrams produced using this model, corresponding to field points E, B, and A. Spots for points C and D are mirror images of those for B and A, respectively. The spot diagrams are produced using 21 rays on a rectangular grid in the pupil, replicating approximately the distribution of rays used in the Hartmann test. The plane object surface coincides approximately with the telescope image surface in points E and B, but in point A, a defocus of about 9mm is introduced. This corresponds to a defocus of 3mm in the instrument focal plane, as can be observed in Figure 10.

NB: When Hartmann tests are to be made on point A during PFM tests, it may be necessary to correct for this defocus to avoid overlapping Hartmann spots.

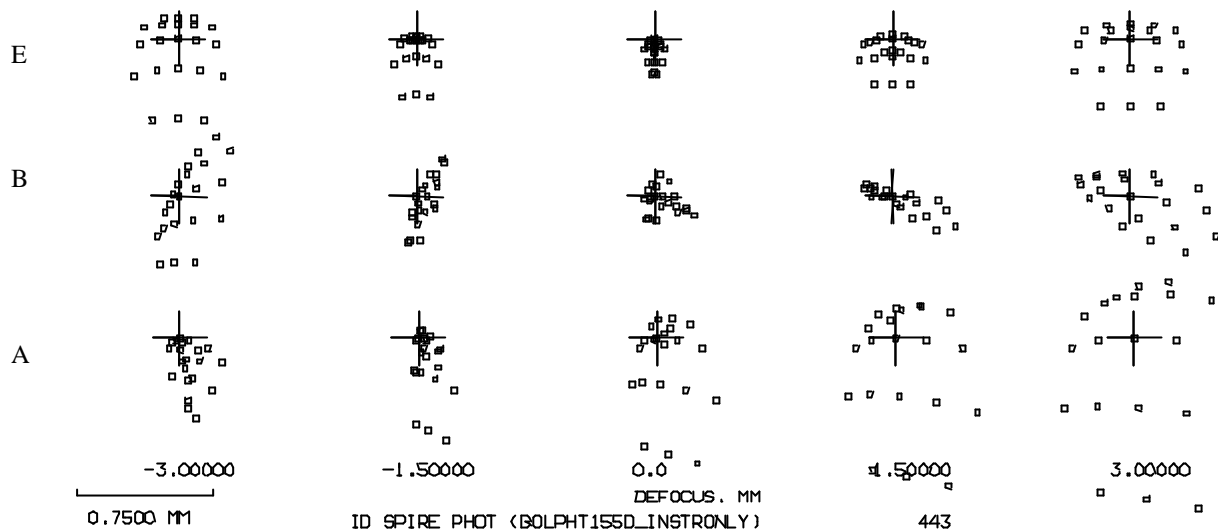


Figure 10. Theoretical through-focus spot diagrams for field points E (upper row), B (middle row), and A (lower row) using the model BolPht155d_InstrOnly in which the instrument object surface is plane. The five columns correspond to moving the SPIRE detector plane axially in steps of 1.5mm. Positive defocus is upstream of the theoretical image plane, ie before the detector surface.

Table 3 lists Zernike coefficients obtained by ratracing for these field points. Signs and order of the coefficients have been corrected to be in agreement with signs and order used in the Hartmann test calculations. The large focus coefficient (Z3) for field point A reflects the departure from the curved image surface. Axial defocus is calculated from the Z3 coefficient by the expression:

$$\Delta = -16 F\#^2 Z3$$

ie, 0.375 Z3 at F/5 and 1.205 Z3 at F/8,68, when Δ is in mm and Z3 is in μm .

Table 3. Theoretical Zernike coefficients in μm for points E, B, and A for the model BolPht155d_InstrOnly in which the instrument object surface is plane.

Zname	Number	SynoZ	InstrOnly_E	InstrOnly_B	InstrOnly_A
			<i>BolPht155d</i>	<i>BolPht155d</i>	<i>BolPht155d</i>
cTiltX	Z1	ZS2	5.02	1.89	9.75
cTiltY	Z2	ZS1	0.00	3.06	3.21
cFocus	Z3	ZS3	-0.32	-0.77	-8.22
cAstX	Z4	ZS4	-1.76	-4.56	5.46
cAstY	Z5	ZS5	0.00	-4.91	-0.48
cComaX	Z6	ZS7	2.47	0.91	4.82
cComaY	Z7	ZS6	0.00	1.53	1.60
cSph	Z8	ZS8	0.24	0.25	0.27
cTri5X	Z9	ZS10	-0.94	-0.47	-1.55
cTri5Y	Z10	ZS9	0.00	-0.34	-0.85
cAst5X	Z11	ZS11	-0.17	-0.14	-0.21
cAst5Y	Z12	ZS12	0.00	0.01	0.02
cComa5X	Z13	ZS14	-0.03	-0.02	-0.04
cComa5Y	Z14	ZS13	0.00	0.00	0.00

6.2. Hartmann results

Figure 11 shows through-focus spot diagrams obtained with the Hartmann test for points E and A. The scale is approximately equal to that of Figure 10, but the spots are rotated 90° anticlockwise. A defocus offset of 1mm has been introduced in the case of field point E, see discussion below. While the spots for Point E correspond well with the theoretical spots, some discrepancy is observed for point B. The Zernike analysis quantifies these differences.

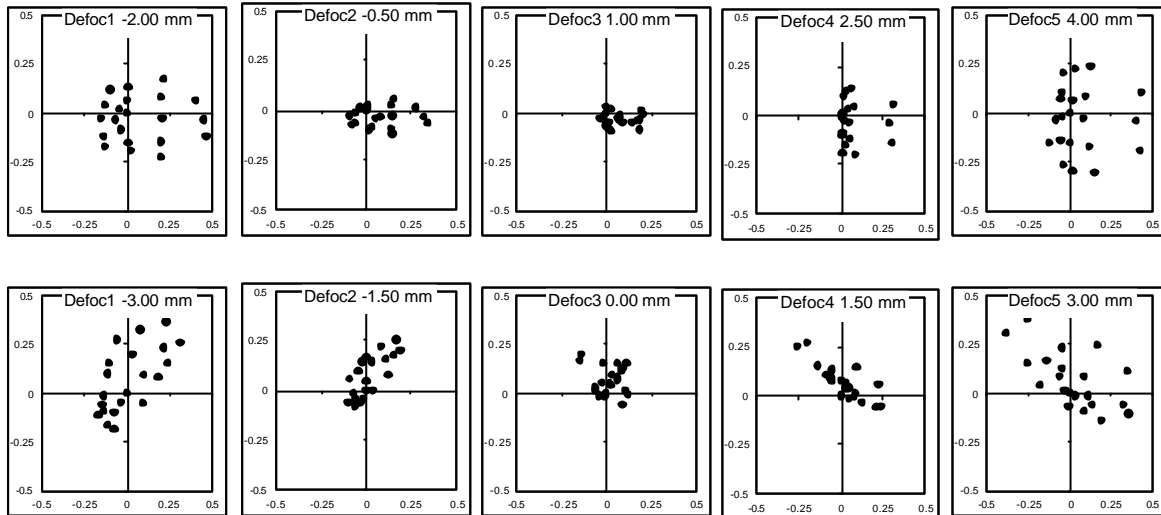


Figure 11. Through-focus spot diagrams obtained from the Hartmann tests for field point E (upper row) and B (lower row). See Figure 10 for explanations.

Table 4 lists Zernike coefficients obtained from the Hartmann test. Comparison with the theoretical coefficients listed in Table 3 indicates differences in most coefficients between 0.15 and 0.45 μm . This is probably representative of the inherent noise level due to cumulative errors in the test method. Although a proper error analysis has not been effectuated, the main error source is expected to be the precision of Hartmann spot coordinate determination. Differences between the theoretical system and the measured results greater than 0.5 μm are also listed in Table 3.

Table 4. Experimentally obtained Zernike coefficients in μm for points E and B.

Zname	Number	SynoZ	PhtSTM_E μm WFE	PhtSTM_B μm WFE	Difference E μm WFE	Difference B μm WFE
cTiltX	Z1	ZS2	4.48	1.58		
cTiltY	Z2	ZS1	-3.21	5.28		
cFocus	Z3	ZS3	-2.51	-0.34	-2.19	
cAstX	Z4	ZS4	2.52	-1.36	+4.28	+3.20
cAstY	Z5	ZS5	-0.15	-5.59		-0.68
cComaX	Z6	ZS7	2.64	0.55		
cComaY	Z7	ZS6	-0.18	1.93		
cSph	Z8	ZS8	0.66	1.17		+0.92
cTri5X	Z9	ZS10	-1.35	-0.85		
cTri5Y	Z10	ZS9	0.30	-0.57		
cAst5X	Z11	ZS11	0.22	-0.21		
cAst5Y	Z12	ZS12	-0.73	-0.15	-0.73	
cComa5X	Z13	ZS14	0.19	-0.18		
cComa5Y	Z14	ZS13	0.22	0.26		

7. Discussion

The 2.19 μm difference in Z3 for point E, corresponding to a defocus of 0.82mm at F/5, is responsible for the focal shift observed in the spot diagrams. This error corresponds to an RMS WFE of $Z3/\sqrt{3} = 1.26\mu\text{m}$, in good agreement with the error budget [RD3] allocation of WFE RMS = 1.15 μm if all mirrors had a relative error of 10^{-3} in their radius of curvature. Although test results indicate that some mirrors are worse than this, the overall effect is similar.

The most important difference concerns the Z4 coefficient, where both points suffer from an increase of about 4 μm , corresponding to $Z4/\sqrt{6} = 1.63\mu\text{m}$ WFE RMS. This error is likely to have three main sources:

- Astigmatic deformation of some mirrors, probably due to stress relaxation
- Differential errors between the two radii of toroidal surfaces
- The definition error of CM3

The definition error of CM3 has been shown [RD4] to be dominated by Z4 = 6 μm (AstX) and Z5 = 21 μm (AstY) on the mirror surface, ie twice as much on a reflected wavefront. However, since CM3 is close to the focal plane, the effect on the image quality is reduced to about 0.5% of this, hence insignificant in this context. The main contribution is probably from astigmatic surface deformations. The error budget [RD3] allocates 2 μm WFE RMS per mirror (ie 1 μm RMS surface error) for a total budget allocation of 6 μm WFE RMS. The measured wavefront error of 1.63 μm is well within this allocation.

The Coma coefficients show good agreement. Coma, which is not easily generated during surface fabrication, is usually an indicator of misalignment errors.

A more compact representation of the Zernike data is given in Table 5. Here, the two terms of non-symmetrical aberrations are root-sum-squared (RSS) to give the total for each term, and each coefficient is multiplied by the corresponding RMS factor (see Table 1). This table therefore shows the contribution to the RMS wavefront error for each term. Total RMS wavefront error at best focus is also shown, as well as corresponding Strehl ratio at 250 μm . The table allows comparison between the theoretical instrument and the as-built instrument.

The final WFE of the as-built model can also be compared with the error budget [RD3], which allocates 8.2 μm WFE RMS to the instrument. With a measured WFE RMS of 2.5 μm at field point B, the SPIRE STM is therefore fully acceptable from the point of view of image quality, including focus.

Table 5. Comparison of RMS coefficients, total RMS wavefront error, and corresponding Strehl ratio at 250 μm for the raytracing model and for the as-built STM.

Aberration	InstrOnly_E	InstrOnly_B	PhtSTM_E	PhtSTM_B
Focus	0.18	0.44	1.45	0.20
Astigmatism	0.72	2.74	1.03	2.35
Coma	0.87	0.63	0.94	0.71
SphAb	0.11	0.11	0.29	0.52
Tri5	0.33	0.21	0.49	0.36
Ast5	0.05	0.04	0.24	0.08
Coma5	0.01	0.01	0.08	0.09
WFE RMS	1.20	2.85	2.10	2.54
Strehl 250um	0.999	0.995	0.997	0.996

SPIRE STM optical alignment campaign

Spectrometer Hartmann test

KD, 15/9/2003

1. Reference documents

- RD1 G. Rousset, "HERSCHEL-SPIRE, SPIRE STM MIRRORS, Optical measurement report", LAS.QUA.SPI.PR.V.030024 Iss1 Rev0, 31/03/2003.
- RD2 K. Dohlen, "Herschel-SPIRE: Optical error budgets", LOOM.KD.SPIRE.2000.002-4, 17/1/2002.
- RD3 K. Dohlen, "SPIRE STM optical alignment campaign, Photometer Hartmann test", 11/9/2003.
- RD4 K. Dohlen, "Herschel-SPIRE: Analysis of 3-D measurements of CM3", 15/4/2003.
- RD5 K. Dohlen, "SPIRE STM optical alignment campaign Estimation of spectrometer beamsplitter tool reflectivity", 1/9/2003

2. Introduction

Measurement of SPIRE image quality is done using a Hartmann test as described in RD3. The test of the spectrometer optics is similar to that of the photometer optics, except only one point in the FOV is measured. However, a D-tool is provided for both detector positions (SSW and SLW, see Fig. 1 a), and, if both beam splitters are in place, each D-tool is seen through the two arms of the interferometer. The Hartmann mask (H-tool) containing a grid of holes is placed in the instrument's internal cold stop pupil, located between SM6 and SM7, where the beam passes through the SPIRE optical bench, see Figure 1 b.

Transverse alignment of the Hartmann lunette with respect to the spectrometer gut ray was done using the MAT. Longitudinal alignment was done using a ruler to measure the distance (e) between the front slide of the Hartmann bench and the upper edge of the SPIRE optical bench along the spectrometer gut ray, as explained in RD3. This distance is given by the equation:

$$e = \text{FFD} + a - d$$

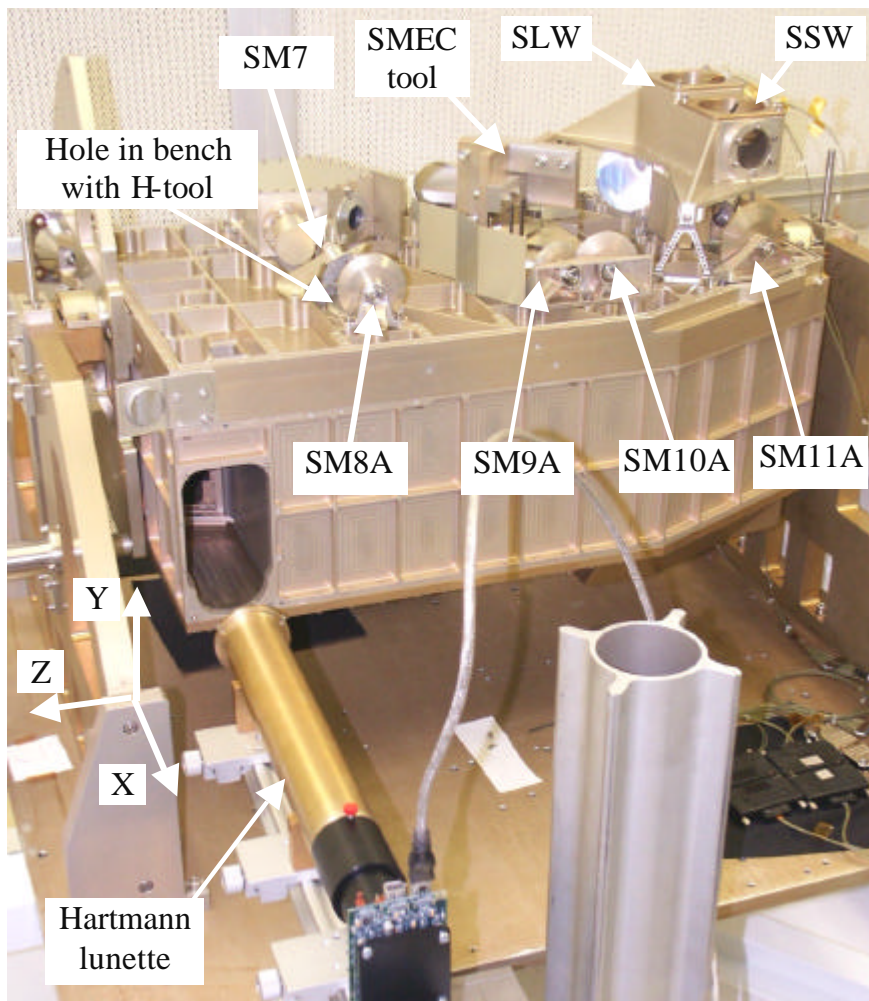
where FFD = 310mm and a = 49.5mm. The distance d, between the upper edge of the Spire bench and the gut ray impact on the Herschel focal surface, is determined by ray tracing (Figure 2). It is 202.303mm cold, ie $d = 202.303 * 1.00415 = 203.14\text{mm}$ at room temperature. Hence $e = 156.36\text{mm}$. Due to some erroneous inputs, the value of e actually used was 157.15mm. The difference of 0.79mm corresponds to $0.4\mu\text{m}$ WFE RMS.

Several factors complicated the STM measurements:

- Only one beam splitter tool was available
- The beam splitter was poorly balanced, with R~90%, T~10% [RD5]
- SM8A had ~12° error in azimuthal rotation due to an error in dowl pin location

The number of observable paths thorough the instrument was limited by the two first problems. The problem of the SM8A rotation was detected and roughly compensated thanks to the Hartmann test. The results of this correction is quantified below. The origin of the problem has since been determined to be due to a faulty bracket and it will be corrected for the PFM.

Three paths through the instrument were used during the tests as shown in Figure 3. These have been denoted SLW_SBS1, SLW_SBS2, and SSW_noSBS. During tests of the PFM, and if both beam splitters are present and have acceptable transmission/reflection characteristics, four paths should be measured by consecutively turning on and off the two D-tools and opening and closing (by insertion of a screen) the upper and lower arms of the interferometer. Table 1 defines the procedure for this and gives appropriate names for each test.



(a)



(b)

Figure 1. a: Setup of the Photometer Hartmann test.
 b: Detail of the Spectrometer Hartmann tool with SM7 (left) and SM8A (right).

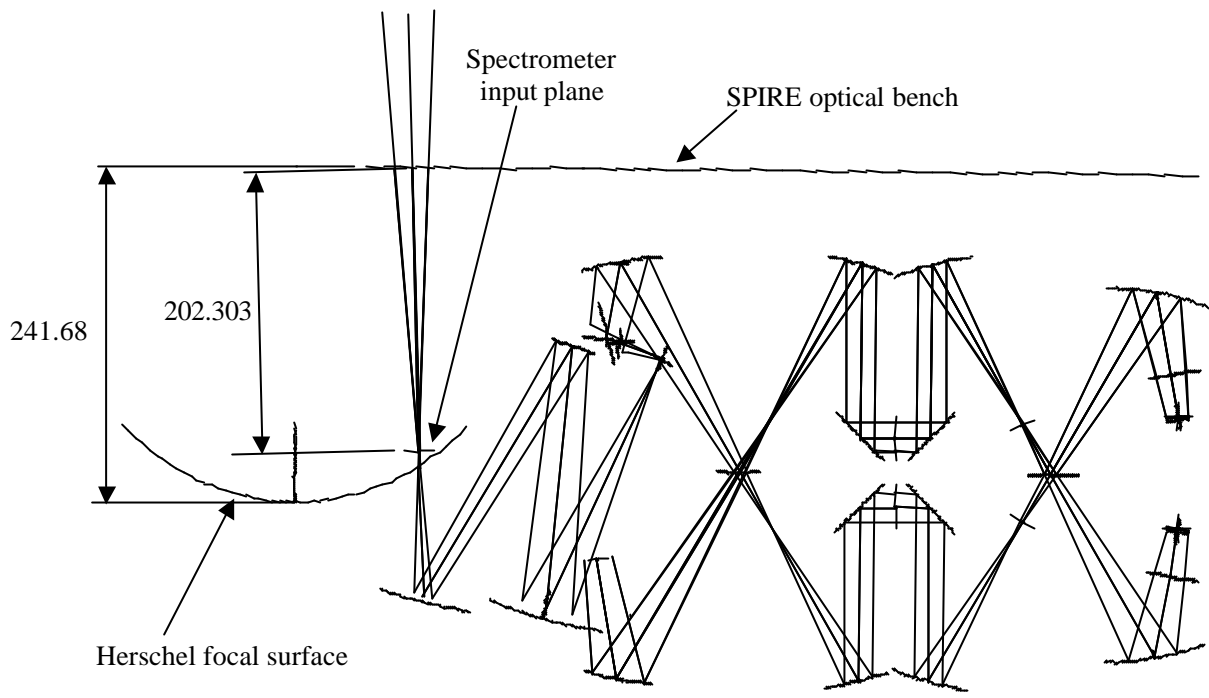


Figure 2. Raytrace diagram showing the position of the spectrometer input plane with respect to the top edge of the SPIRE optical bench. Dimensions are cold (4K).

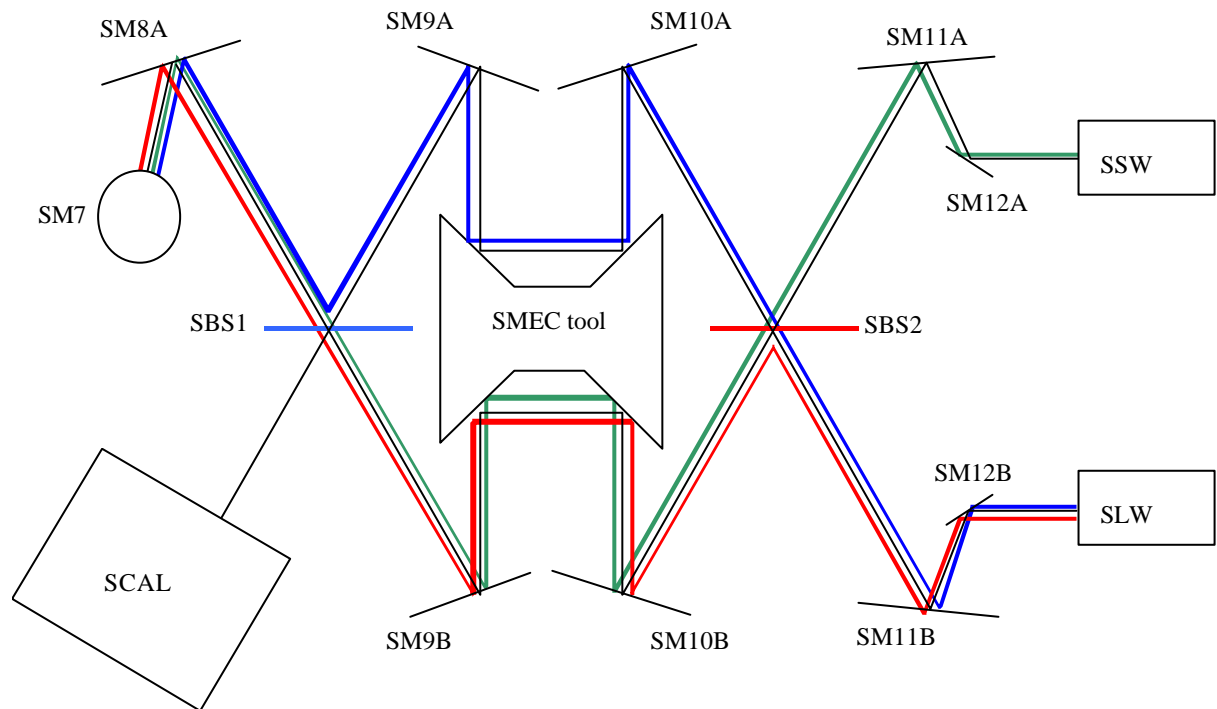


Figure 3. The three beam paths for which Hartmann test was performed: The blue path (SLW_SBS1) realized by placing the beamsplitter tool in the SBS1 position, the red path (SLW_SBS2) realized by placing it in SBS2 position, and the green path (SSW_noSBS) realized by removing the beam splitter.

Table 1. Procedure for measuring the four paths of the spectrometer.

PFM naming	STM naming	SLW	SSW	Upper arm (A)	Lower arm (B)
SLW_A	SLW_SBS1	On	Off	Open	Closed
SLW_B	SLW_SBS2	On	Off	Closed	Open
SSW_A		Off	On	Open	Closed
SSW_B	SSW_noSBS	Off	On	Closed	Open

3. Results

3.1. SM8A rotation

Figure 4 shows a series of images obtained with the Hartmann lunette at 5 different focus positions separated by 9mm in the F/5 Hartmann focus before correction of the SM8A rotation. Clearly, the system suffers from a large amount of astigmatism. At the best focus position (central image), the spot has a diameter of about 230 pixels, corresponding to 1.7mm, almost the size of the Airy disk at 250 μ m whose diameter is 3.0mm. With a separation between astigmatic focal lines of about 20mm, this corresponds to a Zernike astigmatism of 50 μ m or an RMS WFE of 21 μ m. This is twice the total SPIRE error budget and clearly not acceptable for SPIRE science.

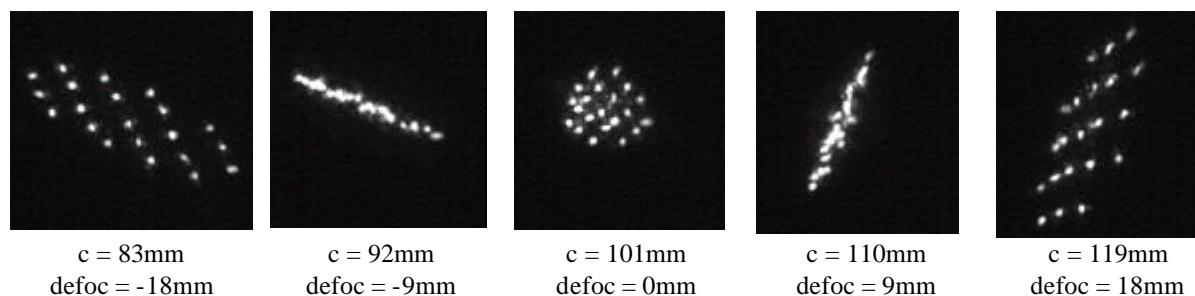


Figure 4. Hartmann through-focus images for the spectrometer in its original as-built configuration.

The optical design prescribes a rotation of the symmetry axis of SM8A through -6.22° around its normal with respect to the instrument axes. The as-built STM turns out to have SM8A rotated by $+6.22^\circ$, ie with an error of 12.44° . Figure 5 shows theoretical spot diagrams produced with this error introduced in the model. The similarity between Figures 4 and 5 is convincing. The Zernike astigmatism of the modified system is 51 μ m.

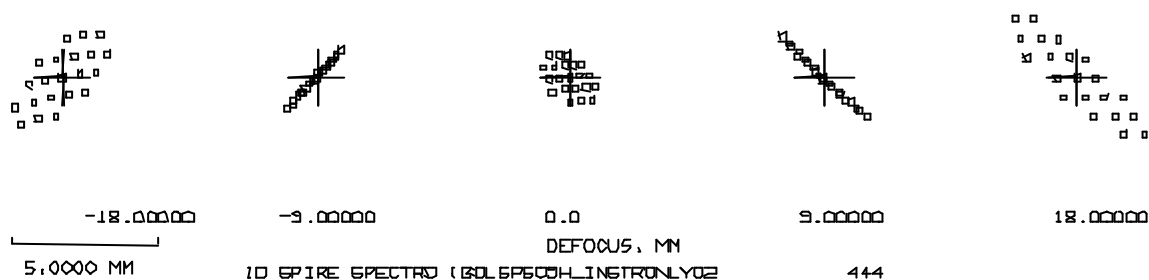


Figure 5. Through-focus spot diagrams produced by ray tracing for a system where SM8A has been rotated in the wrong direction.

After removing the dowling pin, approximate correction of the SM8A rotation was done by rotating the mirror around its spigot axis. No precise means of angular measurement was possible, so the adjustment was done by optimizing the best-focus Hartmann image. Figure 6 shows images taken at approximately 3° intervals near the optimal rotation. The optimum was estimated to be close to image c. Marks were made on the back of the mirror showing the position before and after rotation, see Figure 7. From the photograph, the angle between the two marks is estimated to $15 \pm 1^\circ$ hence 2.5° more than the required 12.44° rotation.

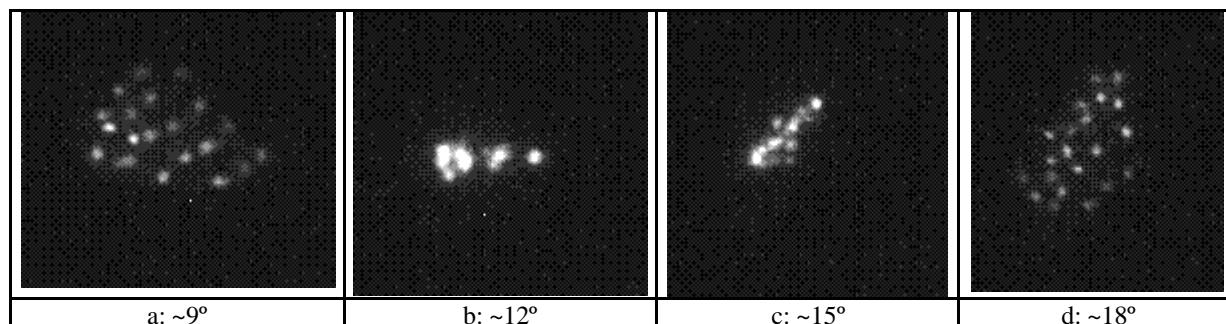


Figure 6. Images taken at approximately 3° intervals near the optimal rotation of SM8A.



Figure 7. View of the back of SM8A showing marks made before and after rotation.

3.2. Through-focus spot diagrams

Hartmann images obtained before rotation of SM8A were too distorted for useful treatment by the Hartmann software. After rotation adjustment, two series of images were taken, corresponding to the paths SLW_SBS1 and SLW_SBS2. Figure 8 shows through-focus spot diagrams produced for both series, compared with spot diagrams produced by raytracing in a system with a SM8A rotation error of 2.5° ($\gamma_{SM8A} = -8.72^\circ$).

Notice that the best image plane of the theoretical model appears to lie some 1.5mm upstream of the theoretical plane. This is due to the fact that the input plane of the "Instrument Only" model was taken to lie on a Herschel image surface assumed to be spherical. In fact it is not, and the difference between the actual telescope focus and the spherical surface is 5.4mm at $F=8.68$, corresponding to 1.8mm at $F=5.0$.

The two series of measured spot diagrams are nearly identical, indicating that the two paths through the interferometer have similar optical performance. They also resemble the theoretical spots (given a rotation of these through 90° clockwise), but there are clearly differences. The Zernike analysis below quantifies these differences.

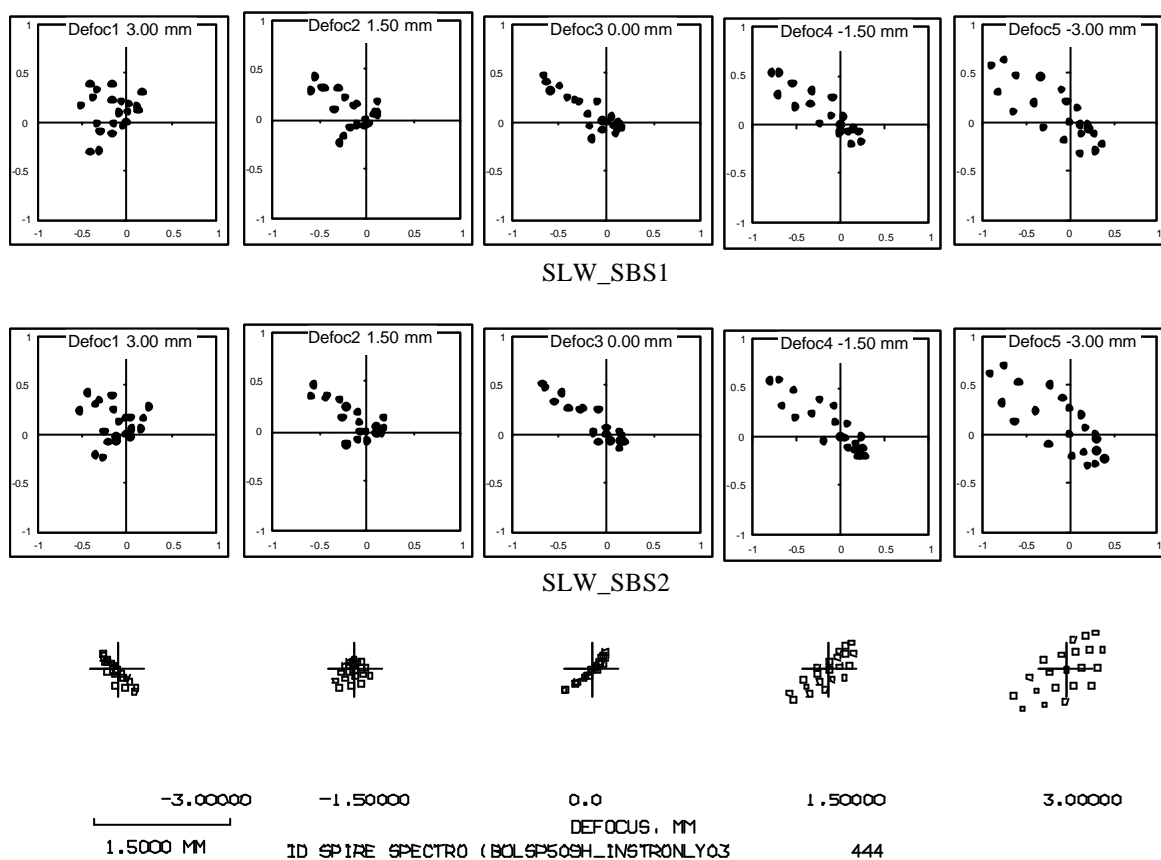


Figure 8. Through focus spot diagrams obtained from the Hartmann rmeasurements (upper and middle row) compared with theoretical spot diagrams for the model including 2.5° rotation of SM8A (lower row).

3.3. Zernike analysis

Table 2 shows Zernike coefficients obtained from the Hartmann measurements, compared with the theoretical coefficients of the ideal instrument (BoISp509h_InstrOnly) and for the case of a 2.5° error in SM8A. The following observations can be made with respect to each aberration type:

Focus:

- The theoretical results have a defocus coefficient of $Z3 = -4.5\mu\text{m}$. This corresponds to 1.8mm image displacement at $F = 5$, as noted above.
- The measured results indicate defocus coefficients of $Z3 = -7.7\mu\text{m}$ and $-9.4\mu\text{m}$, corresponding to 3.1mm and 3.8mm, respectively. The defocus of the instrument is therefore approximately 1.7mm at $F/5$. This corresponds to a WFE RMS of $2.4\mu\text{m}$.

Astigmatism:

- The effect of the SM8A rotation on the theoretical system is only visible on the two astigmatism coefficients: $\Delta Z4 = 6.98\mu\text{m}$ and $\Delta Z5 = 8.01\mu\text{m}$. All other coefficients are equal to within $0.04\mu\text{m}$.
- The measured Astigmatism values are in good agreement with the theoretical system. The mean values of $Z4$ and $Z5$ are within $0.1\mu\text{m}$ and $3.65\mu\text{m}$, respectively, of the theoretical values. The difference in $Z5$ value are probably due to differential errors between radii of toroidal surfaces and astigmatic deformations of some mirrors, as evoked for the photometer.

Coma:

- Both measured paths show non-negligible amounts of coma whereas the theoretical instrument contains very little of this. A sensitivity analysis indicates that this is not easily introduced by misalignments. Interferometric measurements of the mirror SM12A shows that this mirror suffers from $0.9\mu\text{m}$ of Zernike coma on the mirror surface. Since this mirror is very close to the pupil and at 45° incidence, this translates into a Zernike coma on the reflected wavefront of $0.9\mu\text{m} * 2\sqrt{2} = 2.5\mu\text{m}$. As seen in Figure 3, none of the two measurements reported in Table 2 are seen by SM12A. Unless the A and B mirrors have been exchanged during assembly, SM12A cannot therefore be the culprit. However, it shows that coma can be generated during the fabrication process. The mirrors SM8A and SM11A and B, as well as the four flat mirrors used in the SMEC tool roof-top assembly have not been tested and are prime suspects.

Spherical aberration:

- Spherical aberration is also present at a mean level of $Z8 = 1.2\mu\text{m}$. Again, misalignment cannot be considered a source for this amount of aberration. It turns out from the interferometric measurement report [RD1] that both SM9A and SM9B suffers from spherical aberration, with surface Zernike coefficients of $0.74\mu\text{m}$ and $0.67\mu\text{m}$, respectively. Used not far from normal incidence, the wavefront errors induced are close to the double of these numbers, ie $1.5\mu\text{m}$ and $1.3\mu\text{m}$, respectively, in good agreement with the measured results.

Other terms:

- Non-negligible coefficients for treble (Tri5) and 5th order coma (Coma5) are also present. Similar error sources are probable, but the measurement report does not include these aberration terms.

Table 2. Zernike coefficients in μm for the three measurements effectuated on the spectrometer, compared with the theoretical Zernike coefficients.

Zname	Number	SynoZ	BoISp509h InstrOnly	BoISp509h SM8A = 2.5°	STM SLW_SBS1	STM SLW_SBS2
cTiltX	Z1	ZS2	1.63	1.59	-10.60	-7.17
cTiltY	Z2	ZS1	1.05	0.95	9.26	10.16
cFocus	Z3	ZS3	-4.56	-4.51	-7.74	-9.35
cAstX	Z4	ZS4	-1.71	5.27	6.07	4.67
cAstY	Z5	ZS5	3.09	11.10	14.51	15.00
cComaX	Z6	ZS7	-0.82	-0.80	-5.23	-4.80
cComaY	Z7	ZS6	0.53	0.48	1.26	1.59
cSph	Z8	ZS8	0.04	0.04	1.00	1.32
cTri5X	Z9	ZS10	1.73	1.78	0.29	0.71
cTri5Y	Z10	ZS9	-0.42	-0.37	-1.81	-2.45
cAst5X	Z11	ZS11	0.27	0.27	0.25	0.10
cAst5Y	Z12	ZS12	0.12	0.12	-0.43	0.15
cComa5X	Z13	ZS14	0.01	0.01	1.18	0.82
cComa5Y	Z14	ZS13	0.00	0.00	-0.71	-0.54

4. Conclusion

Table 3 compares RMS contributions for each aberration type for each of the theoretical models (as designed and including a 2.5° rotation of SM8A) and the two optical paths measured by the Hartmann test. These numbers include the inherent defocus of the theoretical model and the residual astigmatism error due to SM8A. Still, both measured paths are well within the total instrument error budget allocation of WFE RMS = 10.7μm.

Table 3. Comparison of RMS coefficients, total RMS wavefront error, and corresponding Strehl ratio at 250μm for the raytracing models and for the as-built STM.

Aberration	BolSp509h	BolSp509h	STM	STM
	InstrOnly	SM8A = 2.5°	SLW_SBS1	SLW_SBS2
Focus	2.64	2.61	4.47	5.40
Astigmatism	1.44	5.02	6.42	6.41
Coma	0.35	0.33	1.90	1.79
SphAb	0.02	0.02	0.45	0.59
Tri5	0.63	0.64	0.65	0.90
Ast5	0.09	0.09	0.16	0.06
Coma5	0.00	0.00	0.40	0.28
WFE RMS	3.09	5.70	8.10	8.64
Strehl 250um	0.994	0.979	0.959	0.953